

**Performance Evaluation of Vertically Oriented Compound Parabolic Concentrating
Solar Collector Integrated with Heliostat Field**

By

Suresh A/L Sandrasagar

22743

Dissertation submitted in partial fulfilment of
the requirements of the
Bachelor of Engineering (Hons)
(Mechanical)

JANUARY 2020

Universiti Teknologi PETRONAS

Bandar Seri Iskandar

31750 Tronoh

Perak Darul Ridzuan

CERTIFICATION OF APPROVAL

Performance Evaluation of Vertically Oriented Compound Parabolic Concentrating Solar
Collector Integrated with Heliostat Field


by

Suresh A/L Sandrasagar

22743

A project dissertation submitted to the
Mechanical Engineering Programme
Universiti Teknologi PETRONAS
in partial fulfilment of the requirement for the
Bachelor of Engineering (Hons)
(Mechanical Engineering)

Approved by,



(Assoc Prof Dr. Syed Ihtsham Ul-Haq Gilani)

UNIVERSITI TEKNOLOGI PETRONAS

TRONOH, PERAK

JANUARY 2020

CERTIFICATION OF ORIGINALITY

This is to certify that I am responsible for the work submitted in this project, that the original work is my own except as specified in the references and acknowledgements, and that the original work contained herein have not been undertaken or done by unspecified sources or persons.



SURESH A/L SANDRASAGAR

ABSTRACT

Although there are number of studies to investigate the performance of various CPC design but performance of vertically oriented CPC collectors is not evaluated. The lack of research on the operation of vertical CPC collectors integrated with the heliostat field is another motivation for this research. In order to meet this objective, a CPC collector, consisting of 3 evacuated flow through absorbers need to be set up and integrated with three heliostats at the Solar Research site of Universiti Teknologi PETRONAS, Malaysia. The performance of the CPC collector using water as the working fluid determined by recording and analysing various parameters related to heat transfer. This thesis will therefore experimentally determine the thermal performance and feasibility of thermosiphoning of vertically oriented CPC collectors integrated with heliostat field in Malaysia's climate. From the experiment conducted, it shows that thermosiphoning, was not feasible to be employed in a vertically oriented CPC collector without heliostat field. The water outlet temperature in the collector reach up to 50°C on a day where solar radiation intensity was high. From the experiment conducted on vertically oriented CPC collector integrated with heliostat field, it was determined that thermosiphoning was feasible. The water outlet temperatures reach up to 101°C and 76°C on a day with high and low rate of solar radiation. Average thermal efficiency of vertically oriented CPC collector when integrated with three heliostats approximately to be 12%.

ACKNOWLEDGEMENT

Firstly, I wish to extend my gratitude to the Lord for giving me strength and blessed with the pleasure of learning new knowledge throughout the project undertaken. None of it would have been possible without Him.

I would like to express my heartfelt gratitude to my beloved supervisor, Assoc Prof Dr. Syed Ihtsham Ul-Haq Gilani for continuous support, guidance and incredible patience to assure that the project is finished within the timeline despite being busy with his duties.

I also would like to take this opportunity to thank Mr. Ibrahim Alhassan Hussain and Mr. Javed Akhter and Mr. Rameez for their sincere assistance in providing necessary guidance, data and equipment required for the experiment.

Lastly, I do want to show my appreciation to my caring parent and friends who have supported and encouraged me throughout the project.

TABLE OF CONTENTS

CERTIFICATIONS	i
ABSTRACT	iii
ACKNOWLEDGEMENT	iv
TABLE OF CONTENTS	v
LIST OF FIGURES	vi
LIST OF TABLES	vii
CHAPTER 1: INTRODUCTION	1
1.1 Background of Study	1
1.2 Problem Statement	3
1.3 Objectives and Scope of Study	3
CHAPTER 2: THEORY	4
2.1 Sun-Earth Geometrical Relationship	4
2.2 Climate in Malaysia	5
2.3 Solar Collector	6
2.4 Compound Parabolic Concentrator (CPC)	7
2.5 CPC Collectors	8
2.5.1 CPC Orientation.	9
2.5.2 CPC Performance Enhancement Technique	10
2.6 Evacuated Tube Collector	11
2.7 Heliostat Field Collector	12
2.8 Circulating System	13
CHAPTER 3: METHODOLOGY	15
3.1 Project Flow Chart	16
3.2 Project Phase	17
3.2.1 Experimental Setup	17
3.2.2 Experimentation	29
3.2.3 Post-Experimental Analysis	29
3.3 Project Gantt Chart	30
CHAPTER 4: RESULT AND DISCUSSION	31
4.1 Thermal Performance of the CPC Collector without Heliostats	32
4.1 Thermal Performance of the CPC Collector with Heliostats	33
4.2 Estimated Power Absorbed by Water	37
4.2 Thermal Efficiency	40
CHAPTER 5: CONCLUSION AND RECOMMENDATION	41
REFERENCES	43

LIST OF FIGURES

Figure 2.1	Motion of the Earth around the Sun	4
Figure 2.2	The Location of Cancer and Capricorn Tropics	4
Figure 2.3	East and West Malaysia's annual average solar radiation (MJ / m ² /day)	5
Figure 2.4	Classification of Solar Collectors	6
Figure 2.5	Construction of CPC	8
Figure 2.6	Distinction of Compound Parabolic Concentrator	8
Figure 2.7	Lens-walled CPC structure with air gap	11
Figure 2.8	Evacuated Tube	12
Figure 2.9	Heliostat Field	13
Figure 2.10	Solar Water Heater with Thermosiphon Loop	14
Figure 3.1	Process Flow Diagram of Final Year Project Activities	16
Figure 3.2	Experimental rig	18
Figure 3.3	Field Layout	19
Figure 3.4	Sun Altitude (α) and Azimuth (A) Angles on 13/2/2020	22
Figure 3.5	Sun Altitude (α) and Azimuth (A) Angles on 14/2/2020	22
Figure 3.6	Sun Altitude (α) and Azimuth (A) Angles on 16/2/2020	22
Figure 3.7	Sun Altitude (α) and Azimuth (A) Angles on 17/2/2020	23
Figure 3.8	Elevation (α_{AE}) Angle of East Heliostat	23
Figure 3.9	Elevation (α_{AE}) Angle of Centre Heliostat	23
Figure 3.10	Elevation (α_{AE}) Angle of West Heliostat	24
Figure 3.11	Azimuth (ρ_{AE}) Angle of East Heliostat	24
Figure 3.12	Azimuth (ρ_{AE}) Angle of Centre Heliostat	24
Figure 3.13	Azimuth (ρ_{AE}) Angle of West Heliostat	25
Figure 3.14	Schematic Diagram of Experimental Rig with Location of Thermocouple	29
Figure 4.1	Variation of Water Inlet Temperature, Water outlet Temperature and Water Temperature in Tank with Time on 18 th February.	32
Figure 4.2	Variation of Water Inlet Temperature, Water outlet Temperature and Water Temperature in Tank with Time on 13 th February.	35
Figure 4.3	Variation of Water Inlet Temperature, Water outlet Temperature and Water Temperature in Tank with Time on 14 th February.	35

Figure 4.4	Variation of Water Inlet Temperature, Water outlet Temperature and Water Temperature in Tank with Time on 16 th February.	36
Figure 4.5	Variation of Water Inlet Temperature, Water outlet Temperature and Water Temperature in Tank with Time on 17 th February.	36
Figure 4.6	Estimated Instantaneous Power Absorbed on 13 th February with Water's Mass Flow Rate of 0.001 kg/s and 0.002 kg/s	37
Figure 4.7	Estimated Instantaneous Power Absorbed on 14 th February with Water's Mass Flow Rate of 0.001 kg/s and 0.002 kg/s	38
Figure 4.8	Estimated Instantaneous Power Absorbed on 16 th February with Water's Mass Flow Rate of 0.001 kg/s and 0.002 kg/s	38
Figure 4.9	Estimated Instantaneous Power Absorbed on 17 th February with Water's Mass Flow Rate of 0.001 kg/s and 0.002 kg/s	39
Figure 4.10	Cumulative Power Absorbed by the CPC Collector with Water's Mass Flow Rate of 0.001 kg/s and 0.002 kg/s	39
Figure 4.11	Average Thermal Efficiency of CPC Collector with Water's Mass Flow Rate of 0.001 kg/s and 0.002 kg/s	40

LIST OF TABLES

Table 2.1	Types of Solar collectors and their temperature ranges	7
Table 3.1	Specifications of the CPC collector (Experimental Rig)	17
Table 3.2	The data for declination angle (δ), latitude (Φ) and hour angle (ω) of sun	21
Table 3.3	The target angle (λ) and facing angle (ϕ)	21
Table 3.4	Incident angle (θ) for east heliostat, centre heliostat and west heliostat	25
Table 3.5	Efficiency value for atmospheric attenuation, mirror reflectivity, shadowing and spillage	27
Table 3.6	Calibration Results of PT-100	27
Table 3.7	Gantt chart for FYP 1	30
Table 3.8	Gantt chart for FYP 2	30
Table 4.1	Description of Important Parameters	31
Table 4.2	Maximum water temperature achieved in four days	33

CHAPTER 1

INTRODUCTION

1.1 BACKGROUND

We are blessed an excellent deal of solar power at no value. The most commonly provided sustainable energy supply in the world is solar power. The number of solar power captured by the earth is 5000 times over the amount of all different contributions. Of this number, 30 percent is stored in air, 47 percent is transferred to low-temperature heat and re-radiated to earth, and 23 percent is produced by the biosphere's evaporation/precipitation process. Less than 0.5 percent is reflected in wind and wave kinetic energy and in-plant photosynthetic storage [1].

The radiation incident on the surface of the world will be used inadvisably for the nice of human society. Solar energy is clean, safe and renewable. The Sun gives the earth plenty of solar energy for the betterment of living things [2]. The utilization of solar technology is crucial for each developed and developing countries. Because of increasing energy demand and rising prices of fossil fuels, solar energy is seemed to be a promising source of renewable energy. As a result of the cost of solar energy for humans will be forever and considerably zero. People will expect a cleaner environment and better health by minimizing fuel energy [3].

Solar technology usually consists of two types which are thermal and photovoltaic. The photovoltaic system uses solar cells to converts radiation to electricity, whereas the thermal system uses a solar thermal collector to transform radiation to heat. Such technologies can be found in a wide variety of applications including cooking, drying, waste treatment and heating besides power generation. The solar collectors can be classified based on their thermal application ranging from low to high temperature requirement.

Solar collectors for low-temperature applications are of a non-concentrating form, with a geometric concentration equivalent to one. The collector area is equivalent to the absorber area. In medium and high-temperature applications, two concentrated solar collectors were used where the area of absorber is greater than the area of collector. The flat plate and evacuated tube are highly suited for the solar concentrating purpose of low temperatures [4]. The flat plate type of collector was well known for its simple operating and marginal cost of maintenance.

However, for flat plate collectors, the downside is the fact that solar monitoring is not possible and also the glass top is likely to cause convective heat loss. The evacuated tube collector is thus developed, in which due to the vacuum enclosed within tube it has a higher efficiency compared to flat plate collector. The flat plate collector and the evacuated tube collector are not concentrating and are therefore typically integrated with concentrating solar collector.

There are two forms of concentrated solar collectors available; imaging and non-imaging. Imaging forms of solar collectors involve Parabolic Trough Collectors (PTC), Parabolic Dishes, fresnel and Central Tower. The solar collector for imaging type produces a sun's image at the receiver focal point and sun position needed to be tracked manually by the system. Compound Parabolic Concentrator (CPC) concentrating solar collector which also a non-imaging type. In the case of an optical non-imaging device, it is specified where the optical system will receive the light from a light source instead of the object, then focused on any point of the receiver instead of the image Tracking of the sun is not necessary for this system [6].

1.2 PROBLEM STATEMENT

Many forms of CPC collectors with variations in the designs of reflectors and receivers have been investigated and tested over the years. However, there are very few studies on the performance of vertically oriented CPC collectors. Therefore, there is a need to investigate the performance of such important concentrator while in a vertical position. Also, another motivation for this research is the lack of research on the operation of vertically oriented CPC collectors integrated with heliostat field. However, the drawback when mounting CPC collector in vertical position, there is limitation in receiving solar radiation all day long due to varying sun position. Incorporating a heliostat field with CPC collector expected to increase concentration ratio to compensate for the limitation attained by the system.

1.3 OBJECTIVE

- To experimentally evaluate the thermal performance of a CPC collector integrated with evacuated flow through receivers in vertical position integrated with heliostat field.

1.4 SCOPE OF STUDY

The aim of this project is to study the performance of the compound parabolic concentrator in vertical position integrated with heliostat field. Before starting with the project, a comprehensive literature review is going to be carried out to possess an insight of the working principle, theory and former work concerning the CPC collector and heliostat field. To begin with the project, the experimental rig was set up as per design specification. The performance of the CPC collector integrated with heliostat field collector was experimentally tested to determine the thermal performance of the system in various weather conditions in Malaysia.

CHAPTER 2

LITERATURE REVIEW

2.1 Sun-Earth Geometrical Relationship

The distance from the earth to the sun varies between year and year. At winter solstice (21 December), the minimum distance is $1,471 \times 10^{11}$ m and the maximum is at summer solstice (21 June) around $1,521 \times 10^{11}$ m. The earth-sun distance is $1,496 \times 10^{11}$ m in average throughout the year. The amount of radiation received throughout the whole year varies, mostly in December and also the lowest in June.

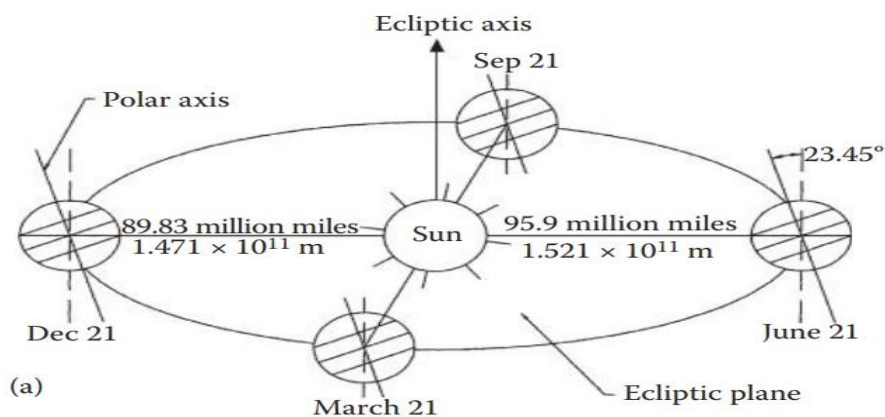


Figure 2.1: Motion of the Earth around the Sun [1]

The earth rotates along its axis in the direction at an angle of 23.45° . This tilt is that the main reason for seasonal variation in the amount of radiation accessible at any places on earth. The angle of the earth-sun line and the plane via the equator is termed as solar declination, δ_s . Declination ranges from -23.45° to $+23.45^\circ$ on 21 December and 21 June. In other terms, the magnitude of declination is the same as the sun's altitude during daytime. The tropics of Capricorne and Cancer are located at acute latitudes. [1]

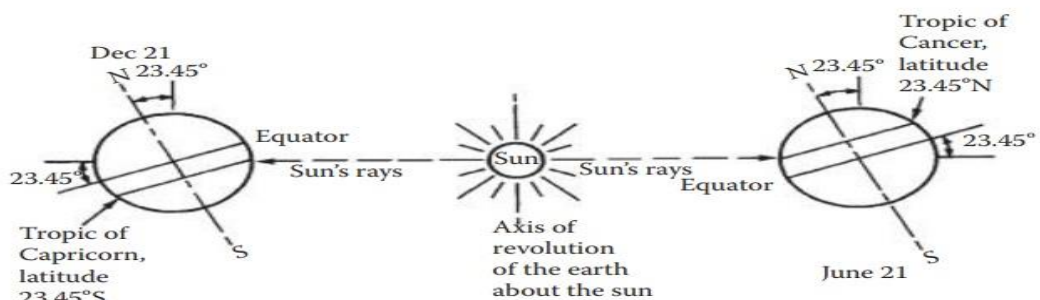


Figure 2.2: The Location of Cancer and Capricorn Tropics [1]

Latitudes over which the sun is not raised at least once a year above the horizon line are described as Arctic and Antarctic. They are arranged at 66 1/2°N and 66 1/2°S individually. Solar Declinations toward the north side of the equator are named positive and those toward the south side as negative. The declination can be determined by the relation.

$$\delta_s = 23.45^\circ \sin[360(284 + n)/365^\circ],$$

Where n is the number of days in the year 1 with n = 1. The decline can be considered constant during any given day for most calculations. [1].

2.2 Climate in Malaysia

Malaysia has an average temperature of 22°C to 33°C all year round and is averaged to 26.5°C. Malaysia is strategically located close to the equator and with the highest solar intake capacity. Malaysia is estimated to have an annual solar irradiation of 400-600 MJ / m². During northeast monsoon the irradiation is intensified where the wind directed from Central Asia to the South China Sea through Malaysia and eventually into Australia between November and March .Lower solar irradiation on the South-West monsoon as the direction of wind varies where it directed from Australia and extends to Sumatera until the Malacca from May to September. Malaysia experiencing a tropical rainforest climate and a range of humidity ranges from 80 to 90 percent except for hills, resulting in highly diffuse radiation due to the dispersion of sunlight in the atmosphere by water molecules [6].

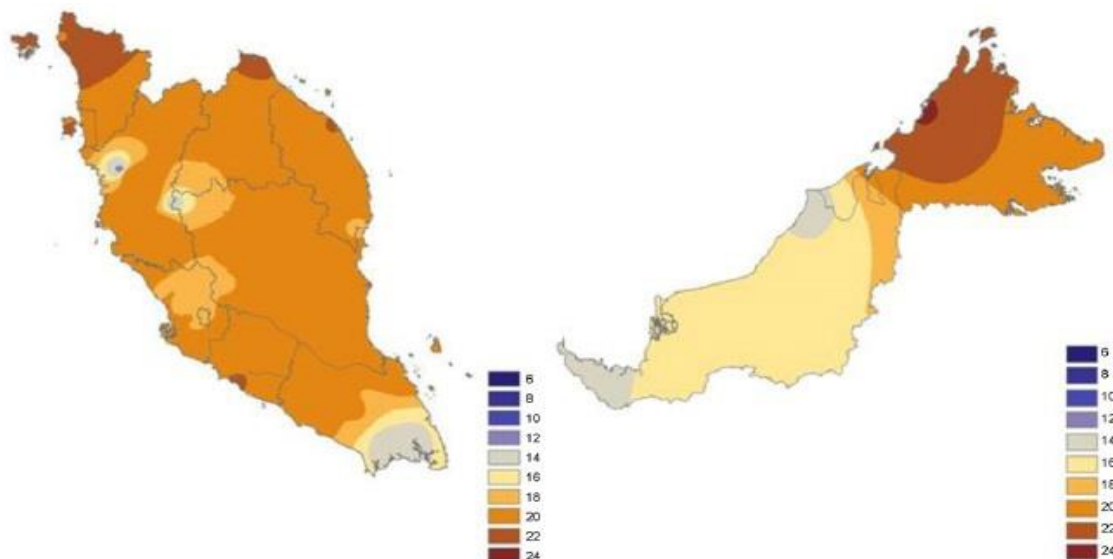


Figure 2.3: East and West Malaysia's annual average solar radiation (MJ / m²/day)

2.3 Solar Collector

A solar collector converts solar irradiation either into thermal energy for solar thermal applications or to electrical energy for Photovoltaic applications. Solar energy is captured as heat by a solar thermal collector and then delivered to its working fluid, which can include either oil, water or air. The heat from the working fluid may also be used for heating household water or for loading thermal power into the storage tank from which the heat is replenished later. A solar panel transforms solar irradiations into electricity for PV applications, besides produces a large volume of waste heat that can then be recovered to fuel through the installation of photovoltaic boards with operating fluids [4].

Solar thermal collectors can generally be classified as two which are non-concentrating and concentrating collectors. The concentrating solar collectors consist of tracking and nontracking collectors. The Compound Parabolic Concentrator (CPC) are concentrating solar collector and non-imaging solar collector where accurate sun tracking is not required.

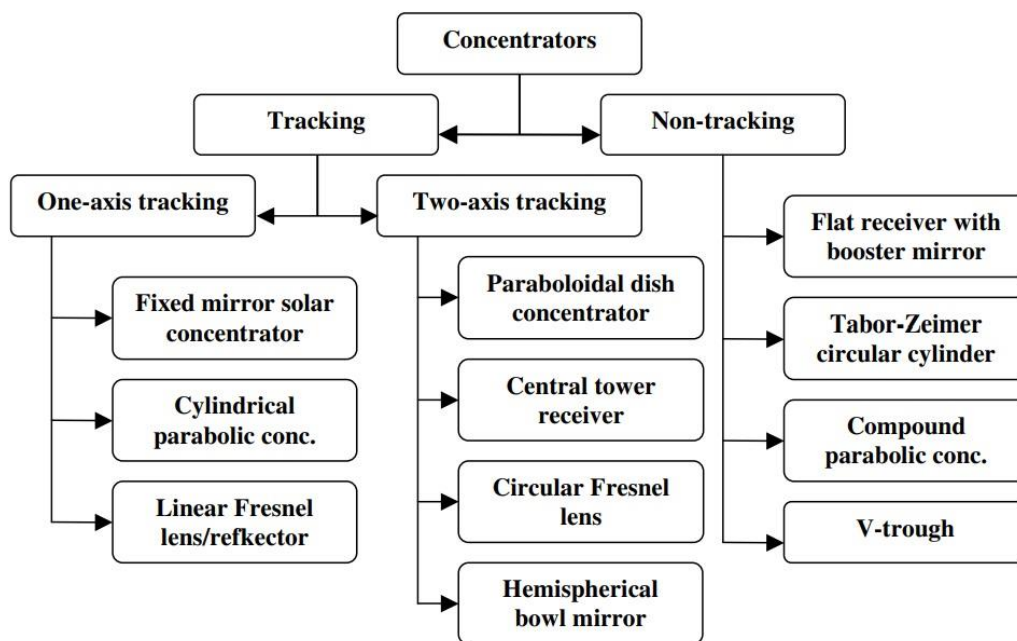


Figure 2.4: Classification of Solar Collectors

Table 2.1: Types of Solar collectors and their temperature ranges

Configuration	Collector	Receiver	Concentration ratio (CR)	Temperature range (°C)
One - axis tracking	Parabolic trough collector	Tube-shaped	10 - 85	60 – 250
	Cylindrical trough collector	Tube-shaped	15 - 50	60 – 300
	Linear Fresnel reflector	Tube-shaped	10 – 40	60 – 400
Two-axis tracking	Parabolic dish reflector	Point	600–2000	100 – 1500
	Heliostat field collector	Point	300–1500	150 – 2000
Stationary	Compound parabolic collector	Tubular	1- 5/ 5 - 15	60 – 240/ 60 – 300
	Evacuated tube solar collector	Flat	1	50 – 200
	Flat-plate solar collector	Flat	1	30 – 80

2.4 Compound Parabolic Concentrator (CPC)

CPC is non-imaging solar concentrators thus having the ability to direct all solar radiation within wide limits to the absorber. CPC has a high efficiency of collecting solar energy [7]. By incorporating two sections of parabola facing with each other, the need to move the concentrator to cater the changing direction of sun may be minimized. According to Figure 2.5, the CPC's half-acceptance angle is a main parameter that negates the need for sun orientation to be tracked by solar tracking devices during the day. The half acceptance angle will be the region at which 90% of rays entering and leaving the receiver. The conventional CPC has an entrance aperture (AB), CPC sides where TIR and reflection occurs and the receiver where the solar absorber is mounted. Incoming radiation accepted relatively within

wide angles by compound parabolic concentrators. With internal reflections radiation projected within CPC's half-acceptance angle reflected to the absorber located at the base.[8]

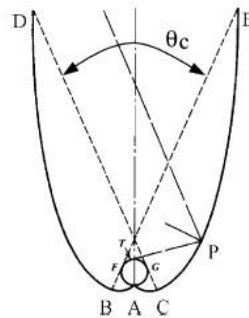


Figure 2.5: Construction of CPC

CPC's orientation depends on its acceptance angle. Figure 2.6 shows multiple geometries of CPC and each acquire different half-acceptance angle. A higher half acceptance angle would have been better to make the maximum gain of solar irradiation from a built CPC, otherwise, the significance of stationary or static will not be met. [8].

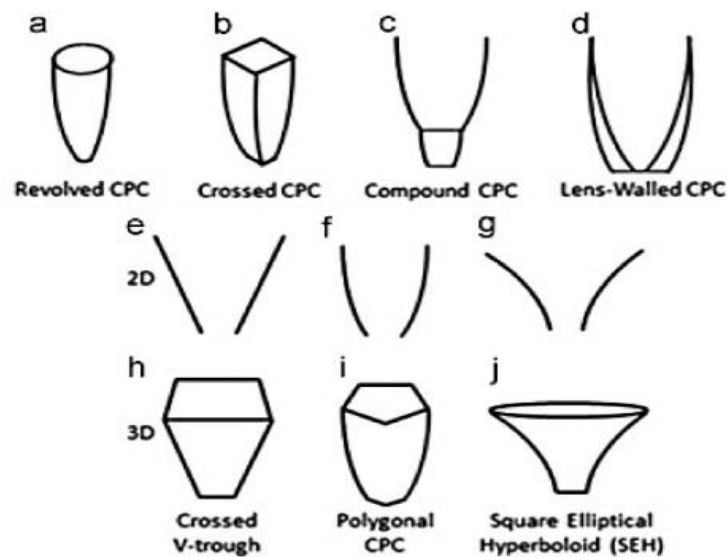


Figure 2.6: Distinction of Compound Parabolic Concentrator [7]

2.5 CPC Collectors

The Compound Parabolic Concentrator (CPC) is a fixed-concentrator radiation concentrator having a moderate temperature (100 - 300 °C) with a low concentration ratios of (1.1X-2X) with reflector intensifying solar radiation up to about 2 - 10 times without Sun

tracker [11]. However, in the case of CPC Collectors with moderate concentration ratios (3X10X), intermediate tracking is required instead of continuous daily tracking as reported by Tian et al.[12] CPC with higher concentration ratios (>10 X - 40,000 X) would be integrated with a solar tracking device to capture maximum solar radiation. Compared to a fixed CPC collector, CPC collector integrated with tracking facilities will produce 14.9% higher efficiency as demonstrated by Kim et al.[13]. However, the sun tracking system requires costly mechanical systems and complicated maintenance for greater thermal efficiency, which make it economically unattractive [11]. Therefore the tracking system has to be used wherever the high concentration ratio is needed to make the collector economically viable and appealing.

2.5.1 CPC Orientation

To maximize radiation intake, solar collector is angled from horizontal. Collectors are usually face at south at a certain angle in to the horizontal in the northern hemisphere and the other way around. This angle is normally referred to as an angle of inclination or tilt, but is called a tilt angle, β throughout this thesis. The tilt is optimized in order to receive enough energy from the solar by both flat and solar concentrating collector at respective location. Several studies conducted to evaluate the radiation gain that may be obtained by tilting a reflector surface by comparing horizontal position. The biggest benefit of a CPC is its high sun-tracking ability due to its wide aperture and half acceptance angle. Even without a tracking device, there will still be some concentration gains. However, to achieve maximum concentration gains, optimum orientation must be chosen [14].

The solar collector's orientation can significantly impact on the solar collector's performance. The solar collector's optimum tilt angle will increase the rate of solar radiation that received by the collector tube significantly. The amount of solar energy absorbed by a collector is influenced by the local solar radiation, view factor, incidence angle modifier and tilt angle for different day. A solar collector in the north hemisphere should be south-faced and north facing if located in the south hemisphere. The yearly optimum tilt angle is suggested to be about $(\phi \pm 15^\circ)$ where plus and minus signs are for winter and summer, respectively [15].

Tang and Wu [16] made the relationship between the monthly radiation received from an inclined surface to find the inclined angle and compared the angle of inclination obtained from the anticipated monthly diffuse radiation with the actual monthly diffuse radiation. Numerous researchers have built up several relations to figure out what is best tilt angle, and created an equation to determine tilt angle from the derivation of total $\cos \theta$. The tilt angle

calculated from the equation was 40° where the answer corresponded to the result of maximum solar radiation received on the 25th of March 2011 at 9.10 am a tilt angle of 30° - 40° at a location in Surabaya, Indonesia. [17].

A study by Khatib et al. [18], finds out the collected yield on an inclined surface is five percent greater than the horizontal surface at five location in Malaysia, using the equation of global and diffuse solar radiation on inclined surface. Malaysia is located at 4.2°N latitude. The sun's position is on Malaysia's Southside from September to March, whereas the sun is on the Northside of Malaysia from April to August. In the present work, the monthly average angle of tilt is calculated using the $\cos\theta$ derivative, which maximizes the value of the $\cos\theta$ and increases the solar radiation received.

2.5.2 CPC Performance Enhancement Technique

In many aspects, the CPC's efficiency can be improved. To optimize radiation collection and reduce energy emissions. Different authors have used various techniques to optimize the collection of radiation and also have an efficient heat transfer medium. In order to reach the goals, it is important to have knowledge on potential failure causes and properties of materials of thermal collectors. The related criteria include the use of different absorbers as receivers, effective selection working fluid and the materials for collector and specific methods for improving overall performance.

Material used by the concentrator may enhance the optical performance and half-acceptance angle due to refractive index [8]. Optical efficiency is the ratio of the solar radiation received at the base of a CPC relative to the incoming solar radiation at the front aperture of the CPC. Increasing the refractive index is considered valid in three dimensional designs, but for two dimensional designs, the optical efficiency of the 3-D designs is not as affected by this enhancement. In terms of acceptance angle, Lens-Walled CPC can improve performance relative to CPC mirror in the same geometric intensity ratio because the lens structure affects the incidence angle direction sunlight. An optical analysis presented by Su et al.[9] shows that lens-walled CPC is more effective in terms of optical performance than the mirror and solid CPC due to the larger acceptance angle and presence of multiple specular reflections. A study conducted by Li et al. [10] shows the air gap present in lens-walled CPC in Figure 2.7 significantly minimize the optical loss and proving that lens-walled CPC with air gap is better than to original lens wall CPC.

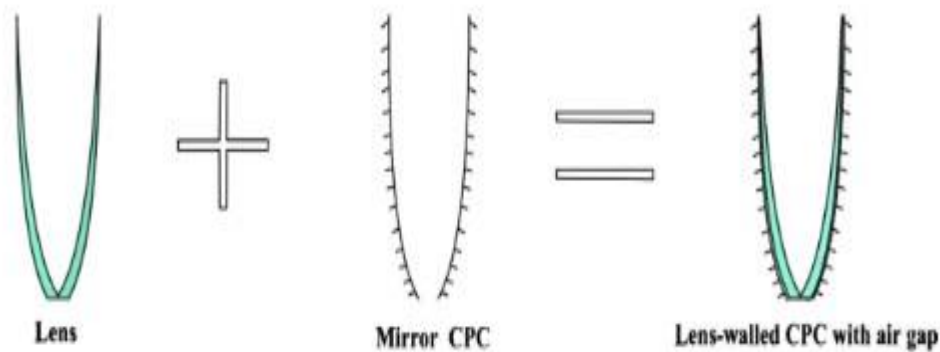


Figure 2.7: Lens-walled CPC structure with air gap [10]

2.6 Evacuated Tubular Collectors

The evacuated tube collector (ETC) is a type of solar collector that enables sunlight to enter via the glass tube and reaches the absorber where heat is being produced. The heat is then being absorbed by the working fluid that flows through the absorber[19]. Gao et al have identified that ETS can be divided into two, one of which is a single-walled evacuated glass tube and the other is a Dewar tube.

This collector's main objective is to avoid heat loss by means of convection and conduction from the internal of the tube collected. This is being achieved by evacuating air from the tube to form a resulting in a lower effect of wind and cold temperatures on the thermal efficiency of the ETC. The cylindrical shape of the evacuated tube able to track the sun all day long in addition to having heat water capacity all year round because of high solar radiation absorption rate.

The limitations of ETC are Evacuated tubes are made of borosilicate glass which are fragile in nature. Extra caution must therefore be taken during the transport or handling of ETC. ETC generates extremely high temperatures so care must be taken during domestic use. ETCs however, are more efficient in industrial applications because they provide water with relatively high temperature. [5]. Thermal performance of water-in-glass evacuated tube using various tilt angles has been studied by Tang et al. The study comprises of experimentation using two different angles 22° and 46° . Study shows there is no significant 12 variation in daily

thermal efficiency. Nevertheless, this study does not give the data for other tilt angles, especially 90° , incorporated with the Compound Parabolic Concentrator.

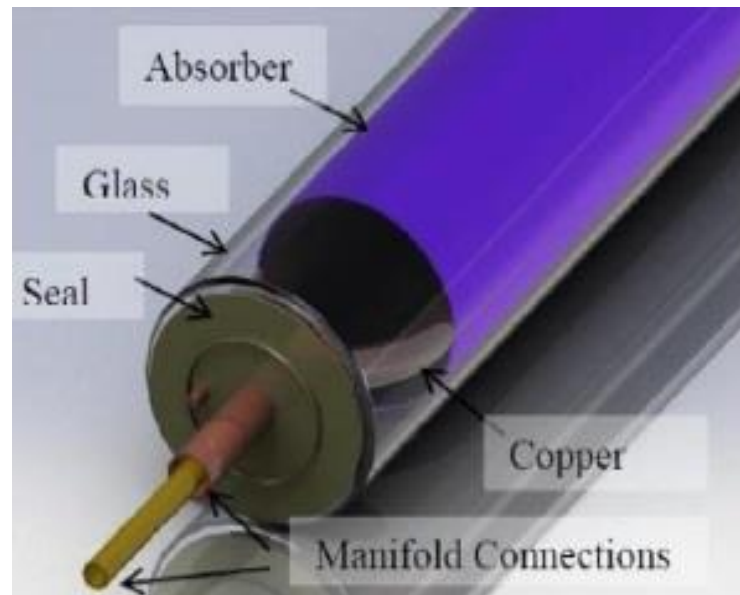


Figure 2.8: Evacuated Tube [11]

2.7 Heliostat Field Collectors

Heliostat Field Collector, known as the Central Receiver Collector, comprises with several flat mirrors or heliostats. Due to the varying orientation of the sun throughout the day, the entire set of heliostats needs to be precisely aligned or oriented to reflect sunlight rays to the common tower. Generally, an automated control system controlled by Altazimuth tracking technology controls the orientation of each individual heliostat. Through the use of an optimized mirror parts which are slightly concave for the heliostats, huge amounts of thermal energy can be directed to the cavity of a steam generator for high temperature and pressure steam production. Therefore, an efficient field architecture model is required to position these heliostats for higher optical performance. Figure 2.9 illustrates how direct Solar radiation incident directed to a common receiver.

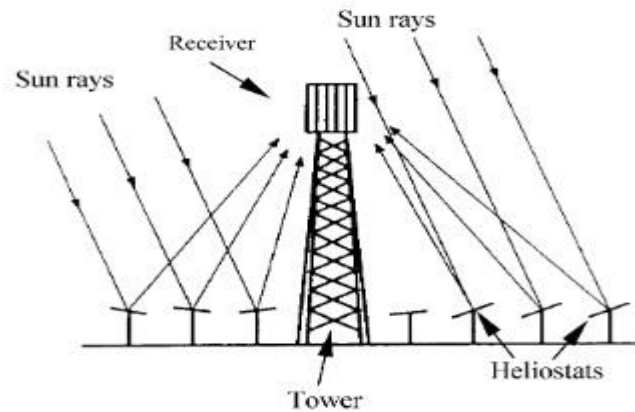


Figure 2.9: Heliostat Field [12]

HFC plants are typically large with estimated output 10 MW and higher. The benefits from an economy scale are required to mitigate this technology's high costs. The solar flux reflected towards the receiver will produce very high concentrations equal to 300–1500 suns because it is incorporated with a large number of heliostats around the central tower. This helps HFC plants to operate for application requiring high thermal requirement [12].

The collector and receiver systems have three common settings. First, the receiver tower is surrounded by heliostats and the heat transfer takes place exterior of the cylindrical receiver surface. Secondly, the heliostats located in the northern hemisphere on the receiver tower and the heat transfer surface of the receiver is enclosed. Thirdly, there are heliostats situated to the north of the receiver tower and there is a north-facing heat transfer surface receiver [12].

2.8 Circulating System

In a thermal solar collector fluid circulating system, The working is heated up and creates a difference in the density as solar heat is absorbed within the collector by the working fluid, which complies with a theory in which higher-density fluids flow below the lower density fluid that produces fluid movement by the collector. A natural circulation is created when the hot water flows from the collector into the water tank, while the lower temperature water moves from the storage tank to the bottom of the collector. The thermosiphon loop in Figure 2.10 is another reference to this natural thermal solar collector fluid circulation. The system is considered passive because of the absence of a mechanical pump. In order for the system to work, the water tank have to be mounted at a location higher than the thermal collector.

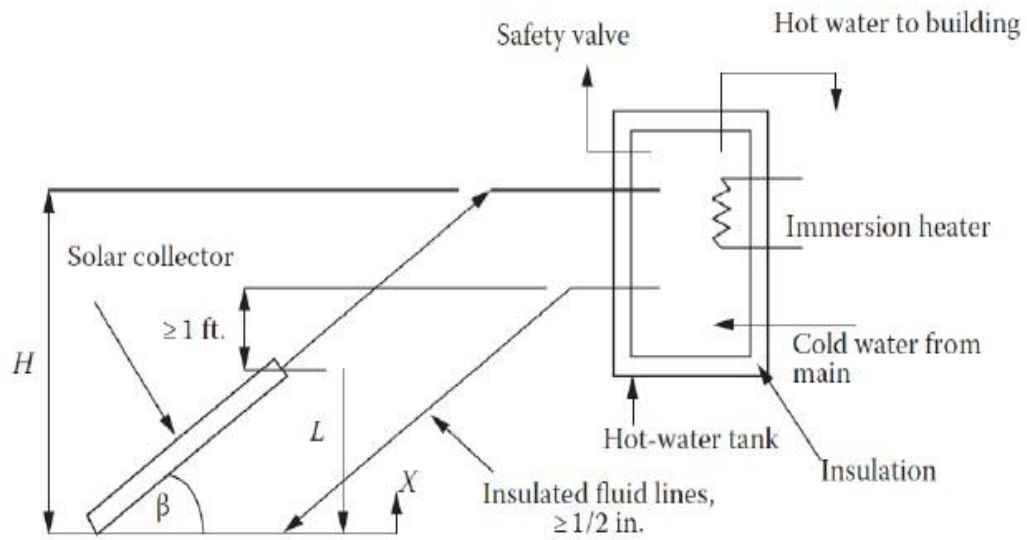


Figure 2.10: Solar Water Heater with Thermosiphon Loop [1]

Goswami [1] stated that the drop in the working fluid flow pressure and pressure change of the buoyant force caused by change in densities of working fluid hot and cold legs must be equivalent:

$$\Delta P_{\text{FLOW}} = \Delta P_{\text{BUOYANT}}$$

$$= \rho_{\text{stor}} g H - \int \rho(x) g dx + \rho g (H-L)$$

In addition, the angle of inclination must be the same as value of latitude. This is because the load changes in the thermal collector system yearly are small. Furthermore, on a sunny day, the difference in temperature between thermal collector's inlet and outlet is normally about 8°C and 11 °C. Besides, the top header of the absorber should be mounted at a distance of at least 30 cm underneath the cold fitting legs of the storage tank. This is to ensure that there is no back flow of water that will cause heat loss surrounding [1].

CHAPTER 3

METHODOLOGY

The chapter is divided into three parts. The first section illustrates the flow chart of the activities of the project. The second part explains the different phases of the project. Finally, the schedule of the project is presented in the form of Gantt Charts.

3.1 Process Flow Chart

Figure 3.1 illustrates the flow chart of the project. Intensive literature review and problem identification have been done. Experimental rig was set up and related instruments was installed during commissioning phase. The experimental rig was exposed to reflected solar radiation by three heliostats mirror arranged radially. Required temperatures for further thermal analysis were recorded using data logger.

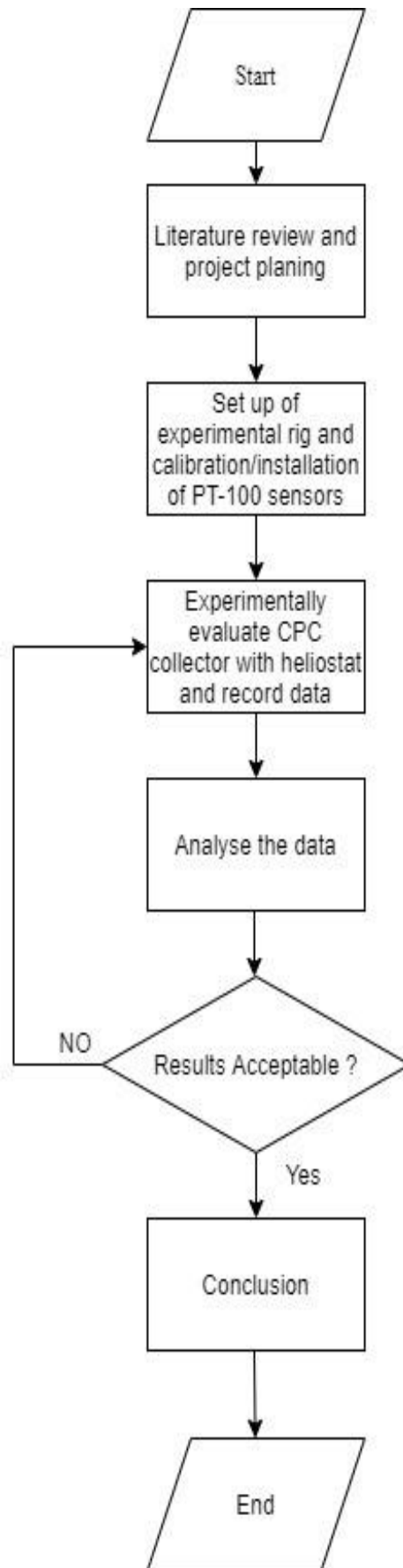


Figure 3.1: Process Flow Diagram of Final Year Project Activities

3.2 Project Phases

3.2.1 Experimental Setup

I. Experimental Rig-CPC Collector

CPC collector coupled with three evacuated flow through absorbers mounted at 90° need to be set up to investigate the thermal performance of the CPC collector and feasibility of thermosyphon. The CPC module was installed with steel frame as supporting base and installed on tower. The tank required for the experiment was fabricated and insulated fairly with fibreglass wool to maintain the temperature of water in the 18 litre tank over long period of time. The connecting pipe was installed prior to minimize heat loss. Water will be used as working fluid for this experiment. The specifications of the CPC collector and the evacuated tubes have been described in Table 3.1 and the experimental rig is illustrated in Figure 3.2.

Table 3.1: Specifications of the CPC collector (Experimental Rig)

Specification	Description
Length of Evacuated Tube	2 m
Width of Evacuated Tube	0.31 m
Inner Diameter of Absorber Tube	36 mm
Outer Diameter of Absorber Tube	40 mm
Outer Diameter of Glass Tube	100 mm
Absorber Material	Stainless Steel
Glass Material	Borosilicate Glass
Absorptivity of Absorber Tube	0.95
Reflectivity of Absorber Tube	0.056
Reflectivity of Mirror	0.9
CPC Half-Acceptance Angle	30°

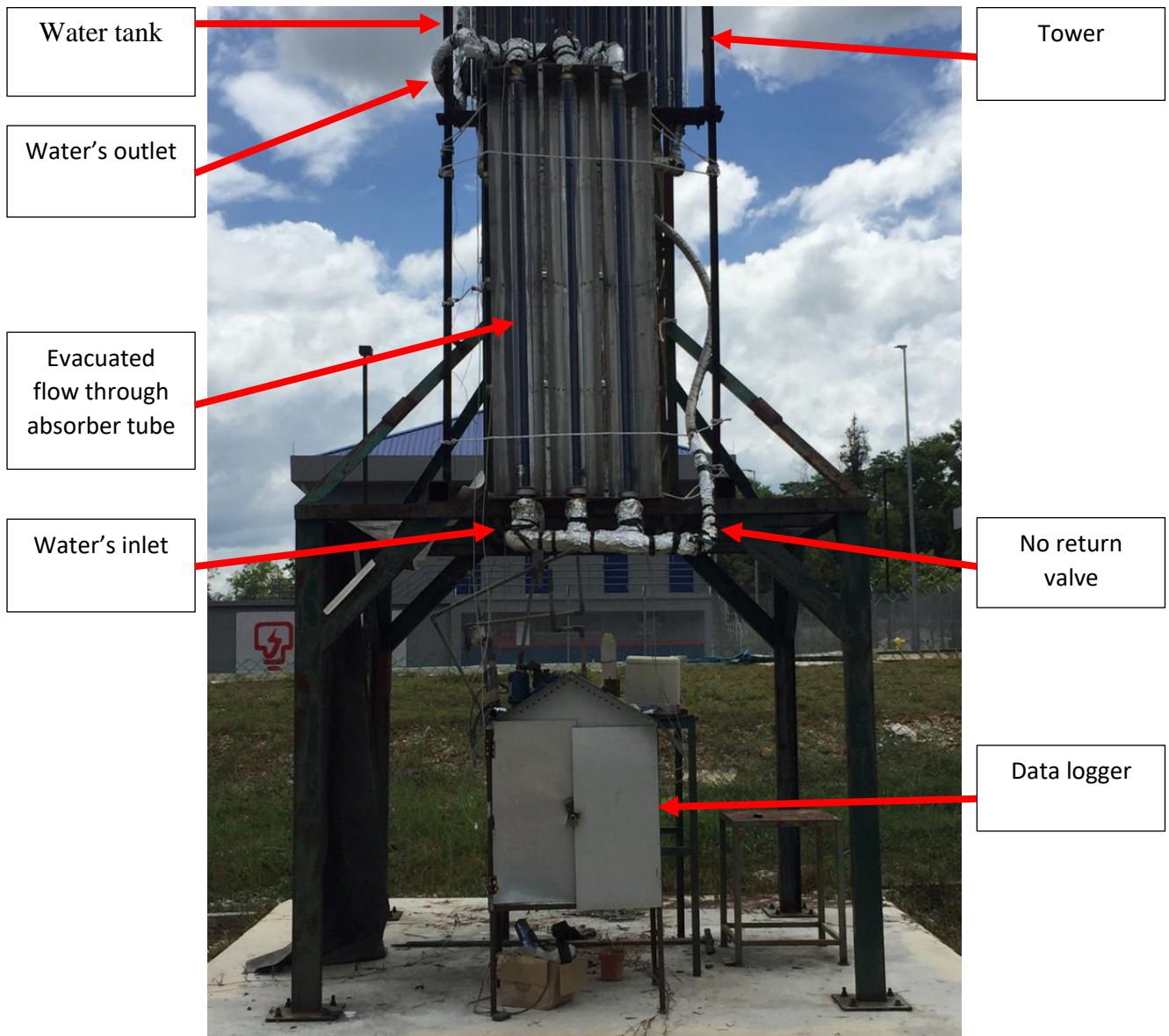


Figure 3.2: Experimental rig

II. Experimental Rig-Heliostat

Heliostat concentrator with 3 mirrors and evacuated flow through absorber tube with tower as shown in Figure 3.2 represent the main components of the system. The distance from centre of three heliostat from the tower is 10.25 meter and the height of each heliostat is 1.5m measure from the ground. The dimensions of each heliostat are 2.5m length and 1.5 m width with aperture area of 3.125m² and total area of 45m². Each heliostat was manually tilted in terms of azimuth angle and elevation angle at interval of ten minutes by focusing the solar radiation onto the fixed target of CPC fixed on the tower. Throughout the tilting process, the

image created upon reflection by heliostat act as reference point to ensure highest available solar radiation exposed to the target point. The field layout is illustrated in Figure 3.3.

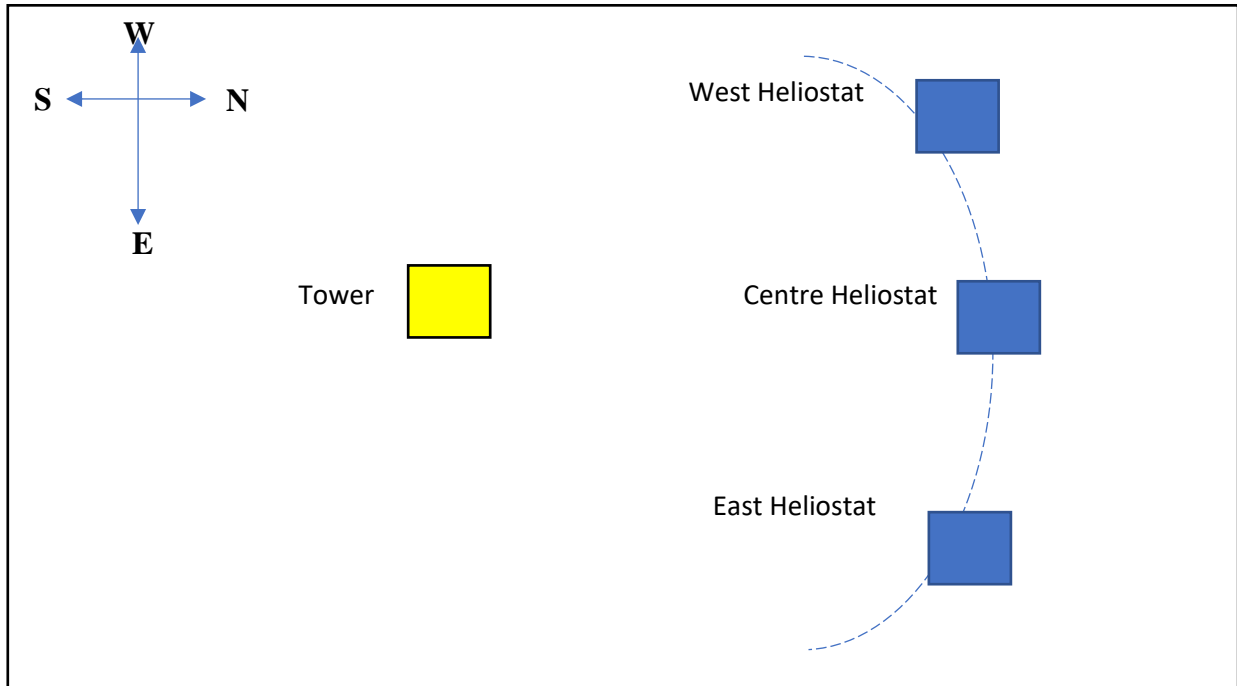


Figure 3.3: Field Layout

In order to complete thermal analysis, the formulas of sun tracking angles for Azimuth Elevation method is used for sun tracking of each heliostat. The AE method is presented in terms of the elevation (α_{AE}) and azimuth (ρ_{AE}) angles as below:

$$\alpha_{AE} = \sin^{-1} \left(\frac{\sin \alpha + \sin \lambda}{2 \cos \theta} \right) \quad (3.1)$$

If $\cos \rho_{AE} > 0$,

$$\rho_{AE}^+ = \left(\frac{\cos \alpha \sin A + \cos A \sin \phi}{2 \cos \theta \cos \alpha_{AE}} \right) \quad (3.2)$$

If $\cos \rho_{AE} < 0$,

$$\rho_{AE}^- = \pi - \rho_{AE}^+ \quad (3.3)$$

Given that,

$$\cos \rho_{AE} = \left(\frac{\cos \alpha \cos A + \cos \lambda \cos \phi}{2 \cos \theta \cos \alpha_{AE}} \right) \quad (3.4)$$

Incident angle is,

$$\theta = \frac{1}{2} \cos^{-1}(\sin \alpha \sin \lambda + \cos \alpha \sin A \cos \lambda \sin \phi + \cos \alpha \cos A \cos \lambda \cos \phi) \quad (3.5)$$

Sun altitude (α) and azimuth (A) angles is,

$$\alpha = \sin^{-1}(\sin \delta \sin \phi + \cos \delta \cos \omega \cos \phi) \quad (3.6)$$

$$A = \cos^{-1} \left(\frac{\sin \delta \cos \phi - \cos \delta \cos \omega \sin \phi}{\cos \alpha} \right) \quad (3.7)$$

Where λ is target angle, ϕ is facing angle, ω is hour angle, δ is declination angle and ϕ is latitude,

The data for declination angle (δ), latitude (ϕ) and hour angle (ω) of sun for 13/2/2020, 14/2/2020, 16/2/2020 and 17/2/2020 is shown in Table 3.2. The target angle (λ) and facing angle (ϕ) for three heliostat is shown in Table 3.3. The sun altitude (α) and azimuth (A) angles are calculated by AE method and illustrated in Figure 3.4, Figure 3.5, Figure 3.6 and Figure 3.7. method. The elevation (α_{AE}) and azimuth (ρ_{AE}) angle for west heliostat, centre heliostat and east heliostat are calculated by AE method and presented in Figure 3.8, Figure 3.9, Figure 3.10, Figure 3.11, Figure 3.12 and Figure 3.13.

Table 3.2: The data for declination angle (δ), latitude (ϕ) and hour angle (ω) of sun

Date	Time	δ	ϕ	Ω
13/2/2020	9 a.m	-13.946	4.3857	-60
	10 a.m	-13.946	4.3857	-45
	11 a.m	-13.946	4.3857	-30
	12 p.m	-13.946	4.3857	-15
	1 p.m	-13.946	4.3857	0
	2 p.m	-13.946	4.3857	15
	3 p.m	-13.946	4.3857	30
	4 p.m	-13.946	4.3857	45
	5 p.m	-13.946	4.3857	60
14/2/2020	9 a.m	-13.62	4.3857	-60
	10 a.m	-13.62	4.3857	-45
	11 a.m	-13.62	4.3857	-30

	12 p.m	-13.62	4.3857	-15
	1 p.m	-13.62	4.3857	0
	2 p.m	-13.62	4.3857	15
	3 p.m	-13.62	4.3857	30
	4 p.m	-13.62	4.3857	45
	5 p.m	-13.62	4.3857	60
16/2/2020	9 a.m	-12.955	4.3857	-60
	10 a.m	-12.955	4.3857	-45
	11 a.m	-12.955	4.3857	-30
	12 p.m	-12.955	4.3857	-15
	1 p.m	-12.955	4.3857	0
	2 p.m	-12.955	4.3857	15
	3 p.m	-12.955	4.3857	30
	4 p.m	-12.955	4.3857	45
	5 p.m	-12.955	4.3857	60
17/2/2020	9 a.m	-12.616	4.3857	-60
	10 a.m	-12.616	4.3857	-45
	11 a.m	-12.616	4.3857	-30
	12 p.m	-12.616	4.3857	-15
	1 p.m	-12.616	4.3857	0
	2 p.m	-12.616	4.3857	15
	3 p.m	-12.616	4.3857	30
	4 p.m	-12.616	4.3857	45
	5 p.m	-12.616	4.3857	60

Table 3.3: The target angle (λ) and facing angle (\emptyset)

Heliostat	\emptyset	Λ
East heliostat	9	158
Centre Heliostat	9	180
West Heliostat	9	202

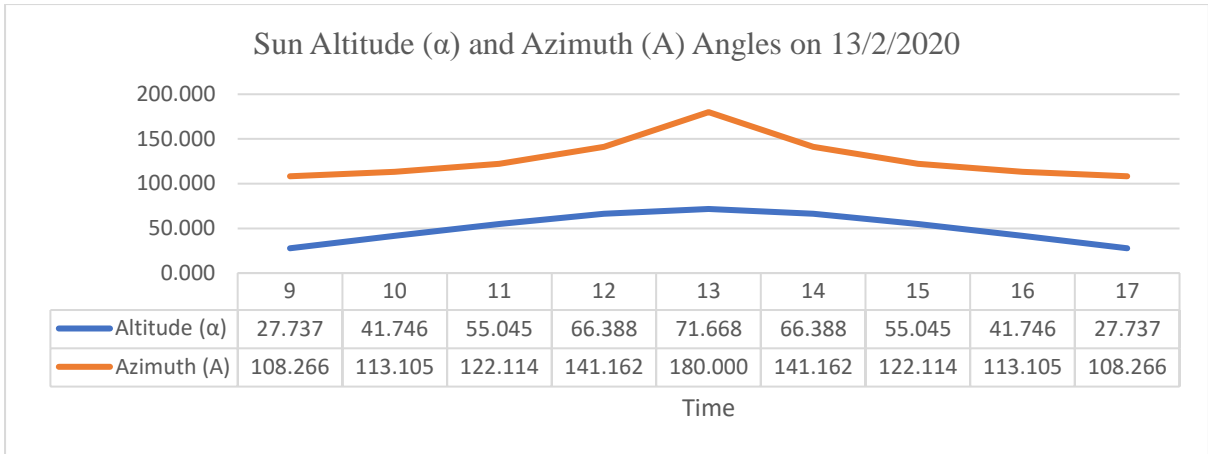


Figure 3.4: Sun Altitude (α) and Azimuth (A) Angles on 13/2/2020

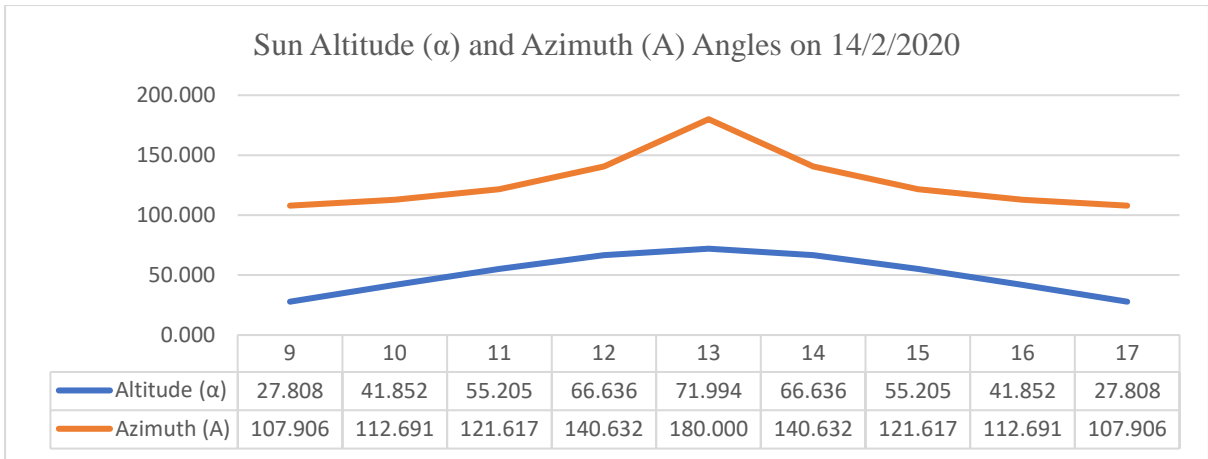


Figure 3.5: Sun Altitude (α) and Azimuth (A) Angles on 14/2/2020

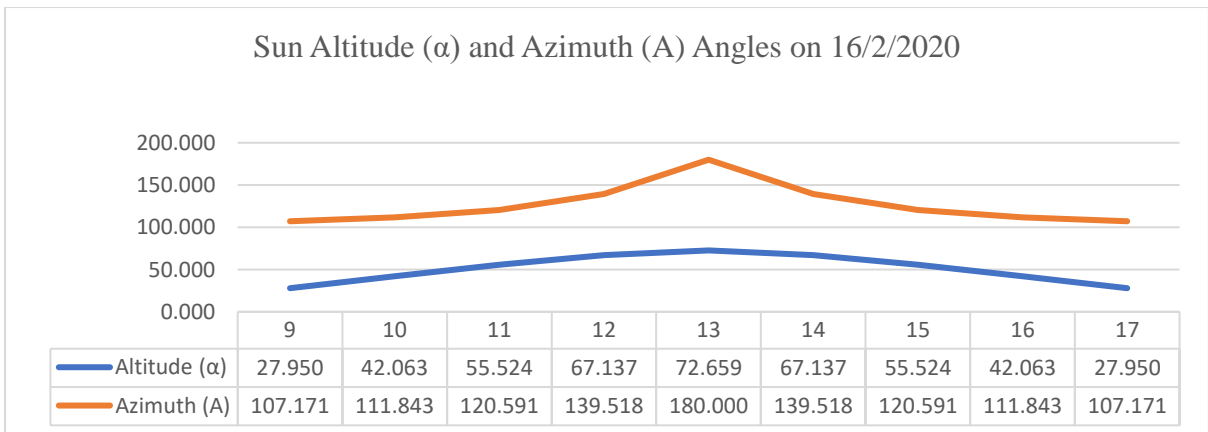


Figure 3.6: Sun Altitude (α) and Azimuth (A) Angles on 16/2/2020

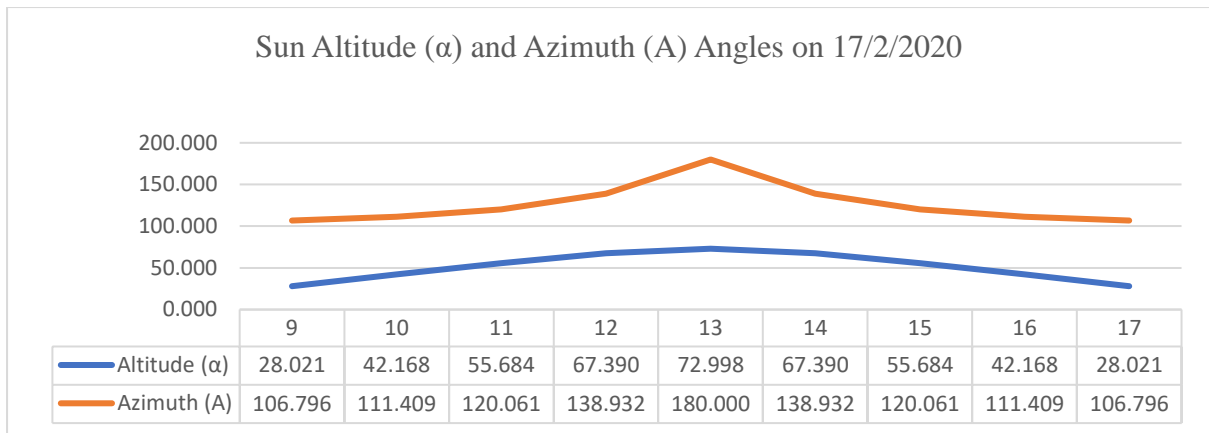


Figure 3.7: Sun Altitude (α) and Azimuth (A) Angles on 17/2/2020

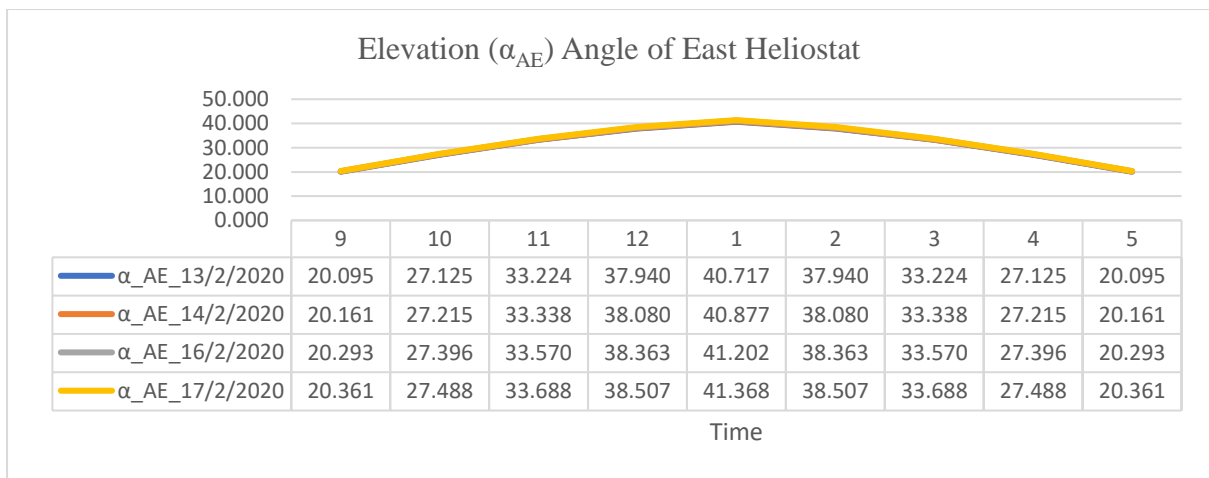


Figure 3.8: Elevation (α_{AE}) Angle of East Heliostat

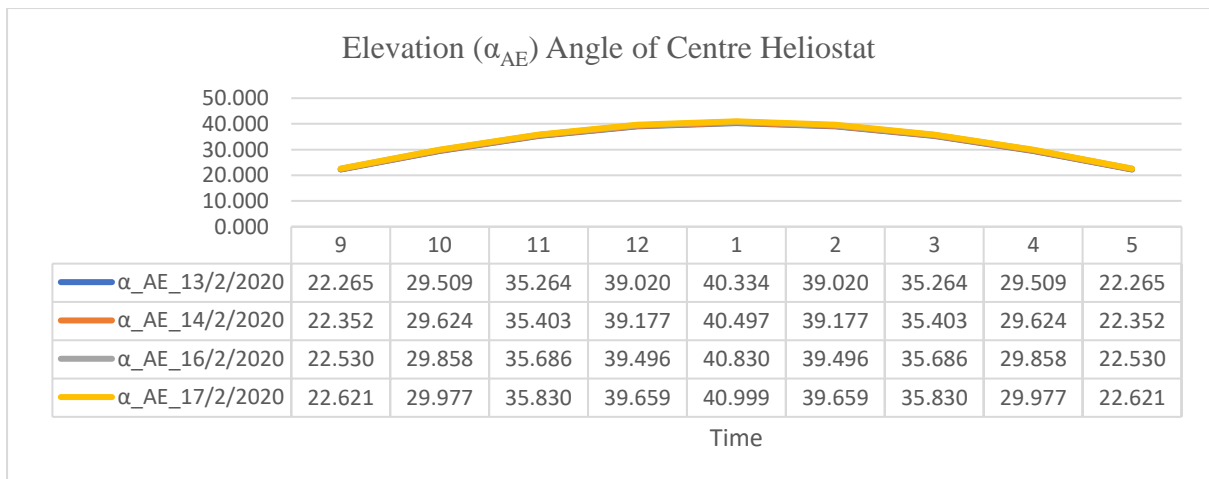


Figure 3.9: Elevation (α_{AE}) Angle of Centre Heliostat

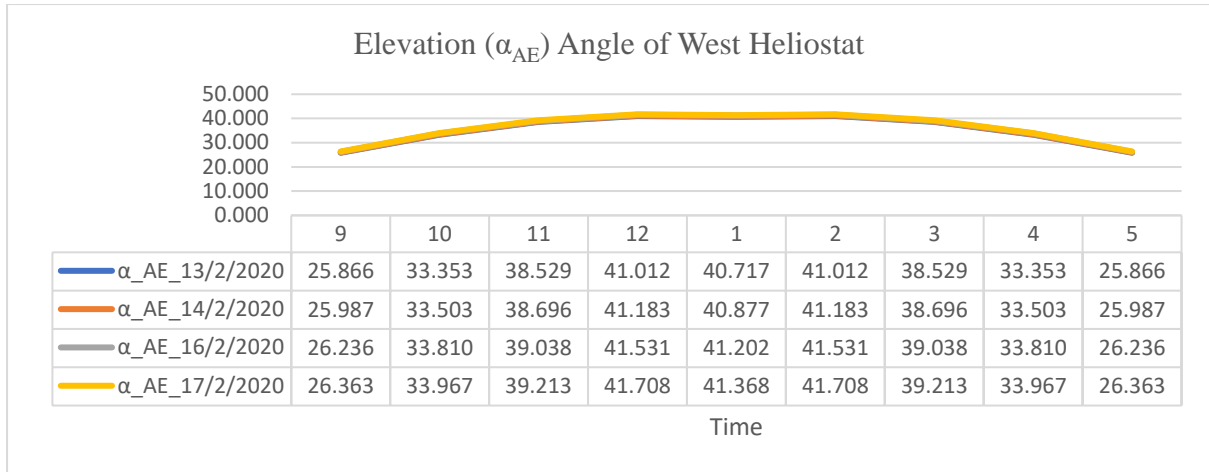


Figure 3.10: Elevation (α_{AE}) Angle of West Heliostat

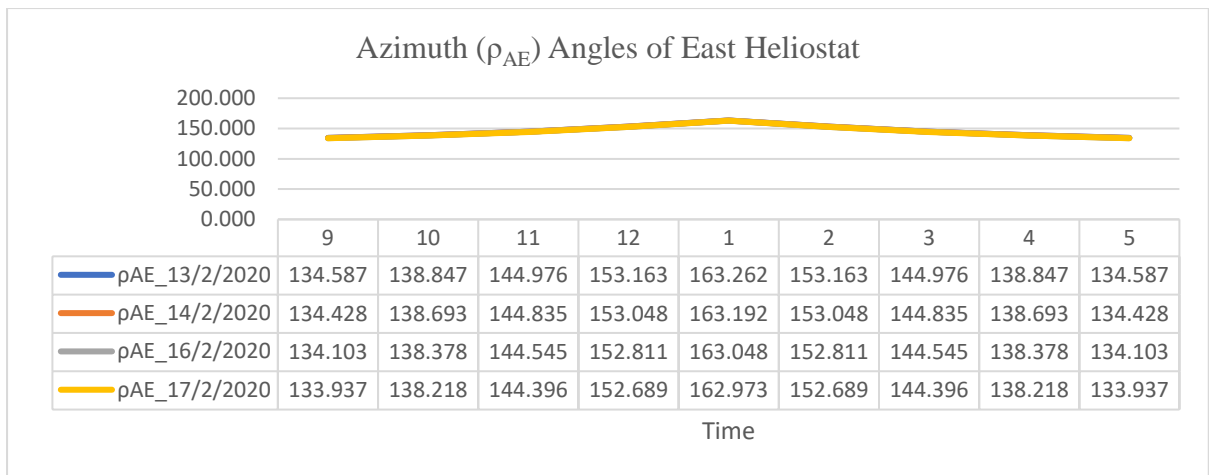


Figure 3.11: Azimuth (ρ_{AE}) Angles of East Heliostat

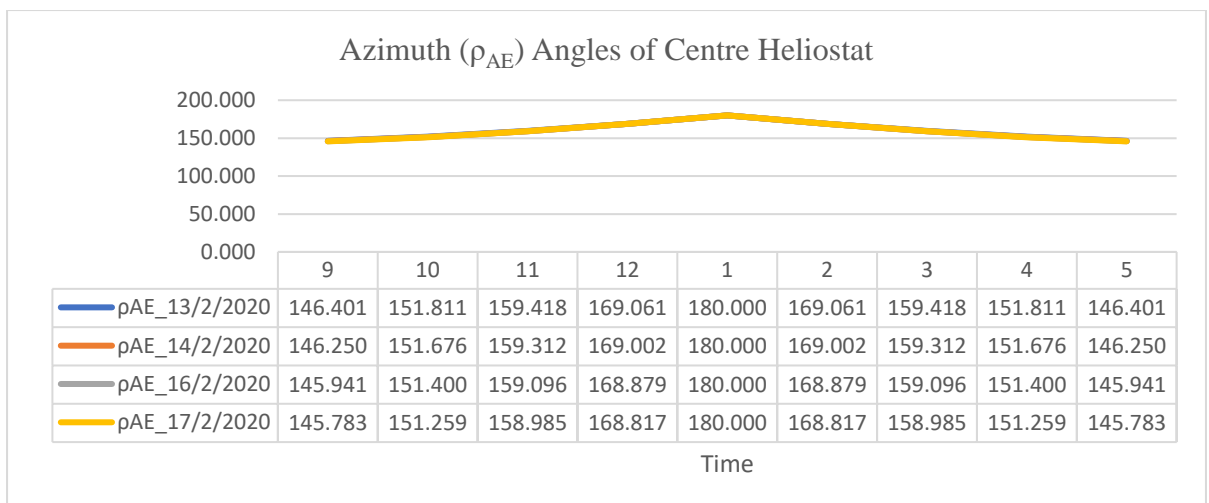


Figure 3.12: Azimuth (ρ_{AE}) Angles of Centre Heliostat

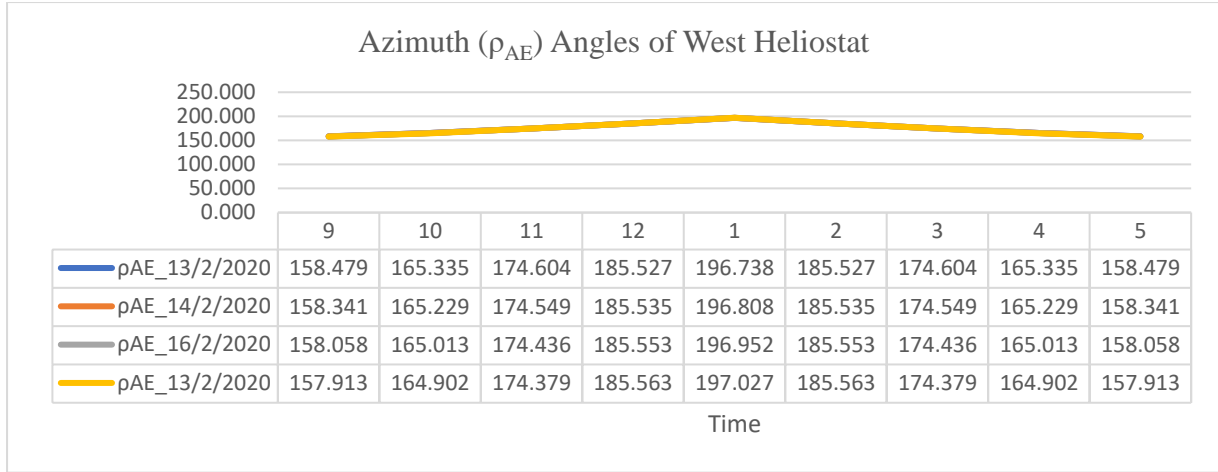


Figure 3.13: Azimuth (ρ_{AE}) Angles of West Heliostat

In order to determine thermal efficiency of CPC collector integrated with heliostat, optical efficiency (η_{opt}), power at the receiver aperture (Q_{in}) determined. The method is expressed as below:

$$\eta_{opt} = \eta_{at}\eta_{ref}\eta_{s\&b}\eta_s\eta_{cos} \quad (3.7)$$

$$Q_{in} = A \times \eta_{opt} \times Irradiation \quad (3.8)$$

Where η_{at} , η_{ref} , η_s , η_{sl} and η_{cos} are atmospheric attenuation efficiency, mirror reflectivity, shadowing, spillage and cosine efficiency. Incident angle (θ) is calculated for η_{cos} and tabulated in Table 3.4. Table 3.4 presents data for η_{at} , η_{ref} , η_s and η_{sl} .

Table 3.4: Incident angle (θ) for east heliostat, centre heliostat and west heliostat

		East Heliostat	Centre Heliostat	West Heliostat
Date	Time	Incident Angle (θ)		
13/2/2020	9	25.18	34.85	44.55
	10	25.62	33.42	41.60
	11	27.04	32.30	38.42
	12	29.27	31.58	35.18
	13	32.06	31.33	32.06
	14	29.27	31.58	35.18

	15	27.04	32.30	38.42
	16	25.62	33.42	41.60
	17	25.18	34.85	44.55
14/2/2020	9	25.35	35.01	44.70
	10	25.78	33.58	41.75
	11	27.20	32.46	38.57
	12	29.42	31.74	35.33
	13	32.21	31.50	32.21
	14	29.42	31.74	35.33
	15	27.20	32.46	38.57
	16	25.78	33.58	41.75
	17	25.35	35.01	44.70
16/2/2020	9	25.68	35.34	45.00
	10	26.11	33.91	42.05
	11	27.52	32.79	38.87
	12	29.73	32.07	35.62
	13	32.51	31.83	32.51
	14	29.73	32.07	35.62
	15	27.52	32.79	38.87
	16	26.11	33.91	42.05
	17	25.68	35.34	45.00
17/2/2020	9	25.85	35.50	45.16
	10	26.27	34.07	42.20

	11	27.68	32.96	39.02
	12	29.89	32.24	35.78
	13	32.67	32.00	32.67
	14	29.89	32.24	35.78
	15	27.68	32.96	39.02
	16	26.27	34.07	42.20
	17	25.85	35.50	45.16

Table 3.5: Efficiency value for atmospheric attenuation, mirror reflectivity, shadowing and spillage

Atmospheric attenuation η_{at}	0.99
Mirror reflectivity η_{ref}	0.89
Shadowing η_s	1
Spillage η_{sl}	0.97

III. Instrumentation

Temperatures at selected position were measured using resistance temperature detector (PT-100). The position of six resistance temperature detector (PT-100) have been illustrated in Figure 3.14 in terms of tag number. Each PT-100 sensors have been calibrated before installation by VITAR-SEGATEC SDN BHD upon Calibration Procedure CP-C. Table 3.6 shows the result of calibration range from 0°C to 180°C at 5 points.

Table 3.6: Calibration Results of PT-100

Tag No	Description	Set Reference Temperature (°C)	Actual Reference Temperature (°C)	Indicated Temperature (°C)	Correction (°C)
1		0	0.3	1.6	-1.3
		30	30.1	28.8	+1.3

	Inlet temperature of water [°C]	70	70	68.9	+1.1
		120	120	119.7	+0.3
		180	180	179.3	+0.7
2	Outlet temperature of water in the East tube [°C]	0	0.3	1.6	-1.3
		30	30.1	28.7	+1.4
		70	70	68.9	+1.1
		120	120	118.9	+1.1
		180	180	179.0	+1.0
3	Outer temperature of water in the Centre tube [°C]	0	0.3	1.0	-0.7
		30	30.1	28.0	+2.1
		70	70	67.7	+2.3
		120	120	118.8	+1.2
		180	180	178.7	+1.3
4	Outlet temperature of water in the West tube [°C]	0	0.3	1.4	-1.1
		30	30.1	28.2	+1.9
		70	70	67.9	+2.1
		120	120	119.1	+0.9
		180	180	179.1	+0.9
5	Average outlet temperature of water [°C]	0	0.3	1.6	-1.3
		30	30.1	28.5	+1.6
		70	70	68.3	+1.7
		120	120	118.3	+1.7
		180	180	179.3	+1.7
6	Temperature of water in the tank [°C]	0	0.3	1.5	-1.2
		30	30.1	28.5	+1.6
		70	70	68.5	+1.5
		120	120	118.7	+1.3
		180	180	179.4	+0.6

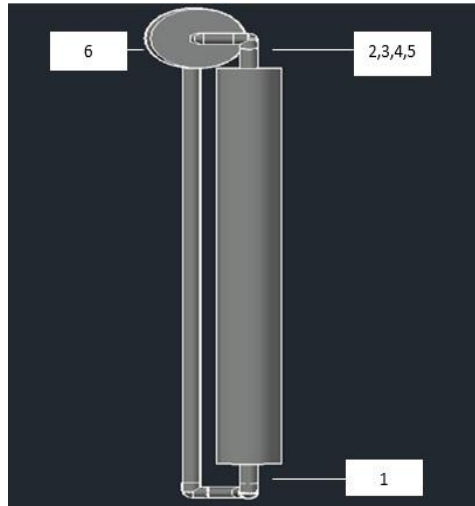


Figure 3.14: Schematic Diagram of Experimental Rig with Location of Thermocouple

3.2.2 Experimentation

Performance of CPC collector will be experimentally performed at Solar Research site in Universiti Teknologi PETRONAS (UTP), Malaysia (4.3857° N, 100.9793°E). The solar collector was tilted to an angle of 90° to allow the incident radiation to be exposed by three heliostats. Water was filled into the CPC collector until the water level above the inlet of tank. Temperature are to measure in several location comprises water's inlet temperature, water's outlet temperature at each evacuated tube and water's temperature in tank to determine important parameter required for further thermal analysis at interval of 2 seconds. Graphtec GL840 data logger was used to logged data. To ensure an optimum water level in the tank, a level gauge was fixed.

3.3.3 Post-Experimentation Analysis

The estimated power absorbed by vertically oriented CPC (Q_{out}) collector will be determined by calculation using heat transfer equation to evaluate if the CPC collector is ideal to be used in such orientation. The thermal efficiency ($\eta_{thermal\ efficiency}$) is calculated. The method is expressed as below:

$$Q_{out} = mc_p(T_o - T_i) \quad (3.9)$$

$$\eta_{thermal\ efficiency} = \left[\frac{Q_{out}}{Q_{in}} \right] \times 100\% \quad (3.10)$$

Where m is mass flow rate (kg/s), T_o is outlet temperature (°C) and T_i is Inlet temperature (°C).

3.3 Project Gantt Chart

Table 3.7. Gantt chart for FYP 1

Phase		Weeks													
		1	2	3	4	5	6	7	8	9	10	11	12	13	14
Problem Identification	Title Selection	█	█												
	Understanding Project Requirements	█	█												
Preliminary Research Work	Literature Review and Problem Identification			█	█	█	█	█	█	█	█	█	█	█	█
	Submission of Extended Proposal						█								
Project Development	Proposal Defence							█	█	█					
	Development of CAD Model								█	█	█	█			
	Submission of Interim Report														█

Table 3.8. Gantt chart for FYP 2

Phase		Weeks													
		1	2	3	4	5	6	7	8	9	10	11	12	13	14
Project Development	Set up of Experimental Rig	█	█	█	█										
	Installation of Instruments and Calibration					█									
	Experimentation, Data Collection and Analysis						█	█	█	█	█	█			
	Documentation									█	█	█	█	█	█

█	Progress	█	Project Milestone	█	FYP Milestone
---	----------	---	-------------------	---	---------------

CHAPTER 4

RESULT AND DISCUSSION

This chapter shows the results obtained from the experimentation. Important parameters tabulated in the graph are indicated in Table 4.1.

Table 4.1: Description of Important Parameters

Tag name	Description
W_i	Inlet temperature of water [°C]
Wo_E	Outlet temperature of water in the East tube [°C]
Wo_C	Outer temperature of water in the Centre tube [°C]
Wo_W	Outlet temperature of water in the West tube [°C]
Wo_avg	Average outlet temperature of water [°C]
T_Tank	Temperature of water in the tank [°C]
Irradiation	Irradiation [W/m ²]

4.1 Thermal Performance of the CPC Collector without Heliostats

Figure 4.1 illustrates the recorded temperatures of vertically oriented CPC collector without heliostats on 18th February. The weather was cloudy in the morning and high radiation experienced in the afternoon. The trend in water temperature namely water's outlet of east tube, water's outlet for centre tube, water's outlet for west tube increased as day progressed. The collector achieved a maximum temperature of 50°C at 3 pm where high solar experienced approximately until 1pm to 3pm. It is also an evident that thermosiphoning was not feasible in such orientation when there are no heliostats integrated because there is no change in water tank temperature throughout the day.

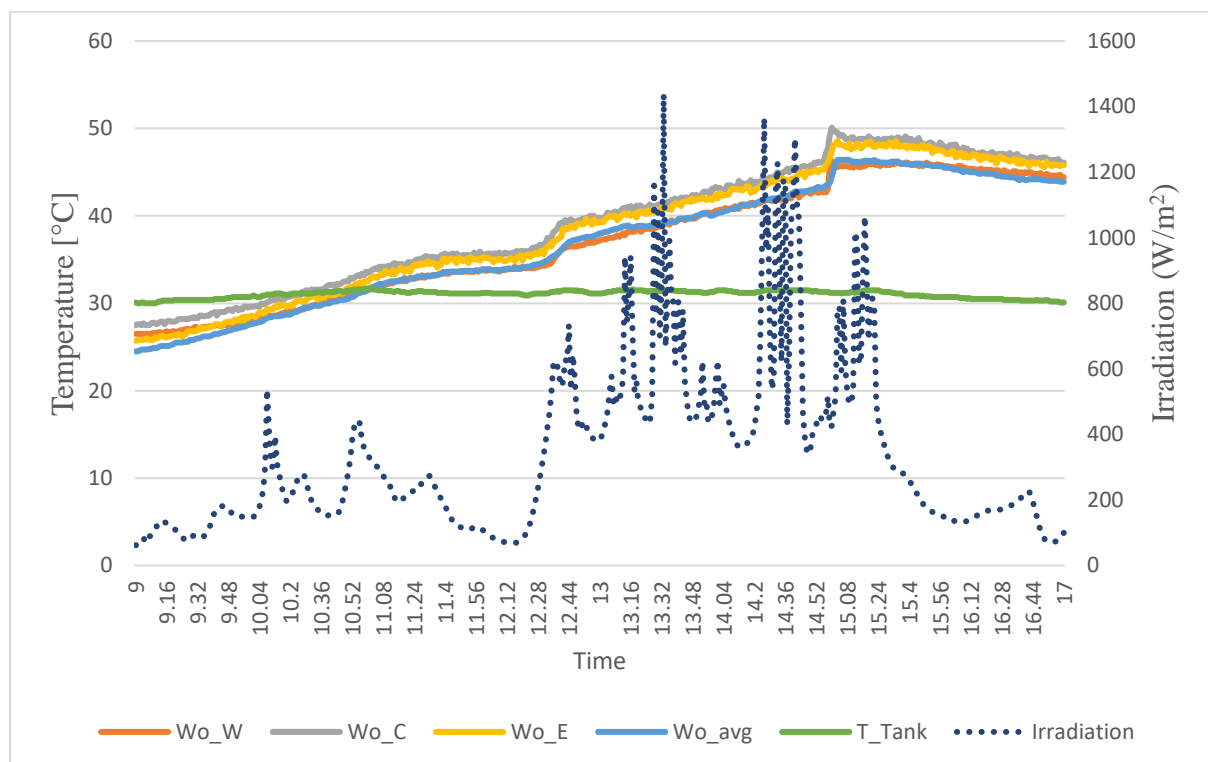


Figure 4.1: Variation of Water Inlet Temperature, Water outlet Temperature and Water Temperature in Tank with Time on 18th February.

4.1 Thermal Performance of the CPC collector with Heliostats

The weather on 13th, 14th, 16th and 17th February were fairly different as the intensity of solar radiation experienced by the solar collector were different over time throughout the day. The weather on 13th February 2020 (Figure 4.2) was sunny and average radiation was experienced throughout the day. The weather on 14th February 2020 (Figure 4.3) was cloudy in the morning and it rained in the afternoon. The weather on 16th February 2020 (Figure 4.4) and 17th February 2020 (Figure 4.5) was mostly sunny and average radiation experienced throughout the day.

The CPC collector is subjected to solar radiation over period of time allowing water to absorb heat energy. The temperature of water's inlet, water's outlet of east tube, water's outlet for centre tube, water's outlet for west tube and water's tank temperature rise as the day progressed depending on the solar radiation reflected by three heliostats. The inlet temperature of water changes with the temperature of water in the tank. Sudden increase in water's inlet temperature found in Figure 4.2, Figure 4.3 and Figure 4.4 are caused by reversed flow of hot water from three absorber tube namely west tube, centre tube and east tube. The maximum water temperature achieved by the vertically oriented CPC collector was tabulated in Table 4.2. The data presented proved that the vertically oriented CPC collector able to function efficiently when integrated with heliostat field.

Table 4.2: Maximum water temperature achieved in four days

Date	Maximum Water Temperature (°C)
13 th February 2020	100.9
14 th February 2020	86.3
16 th February 2020	100.9
17 th February 2020	75.9

From Figure 4.2, Figure 4.3, Figure 4.4 and Figure 4.5, it proves that movement of working fluid (water) inside the CPC Collector is not affected by the inclination angle when integrated with heliostat field. The changes in temperature of water in the tank was used as the primary way to determine the feasibility of thermosiphoning. The water undergone expansion upon absorbing heat energy and flow from the top of the absorber tube into the water tank. This overflowing from the top of the absorber tube into the water tank will induce a natural

circulation as it is a closed system. The temperature of the water in the tank will increase when the hot water flows into the water tank and consequently the temperature of the water at the inlet will also increase significantly over period of time.

Figure 4.4 and Figure 4.5 were an evident that the incident angle of solar radiation significantly effects the amount of energy absorbed by the individual absorber tube namely east, centre and west. By referring to the trend, the water temperature in west tube takes the lead in the morning whereby the water temperature in east tube takes the lead in the afternoon. This is because heliostat fall in the east side to the CPC collector has the highest efficiency. and the amount of solar radiation accepted by west absorber tube is the maximum. For afternoon, the heliostat that fall in the west side to the CPC collector is highest and the amount of solar radiation accepted by east absorber tube is the maximum.

Figure 4.2, Figure 4.3, Figure 4.4 and Figure 4.5 present an evident that tank stratification occurs between 12 to 2 pm. There was a sudden change in tank temperature (T_{Tank}) of different depth of water in the tank as a result of different density of water in the tank. Cold water is denser compared to hot water as it will stratified at bottom of the water tank. The applied heated water from the outlet of the collector resulting from thermosyphon to the top of the tank and drawing cold water from the bottom of the tank to the inlet of the collector.

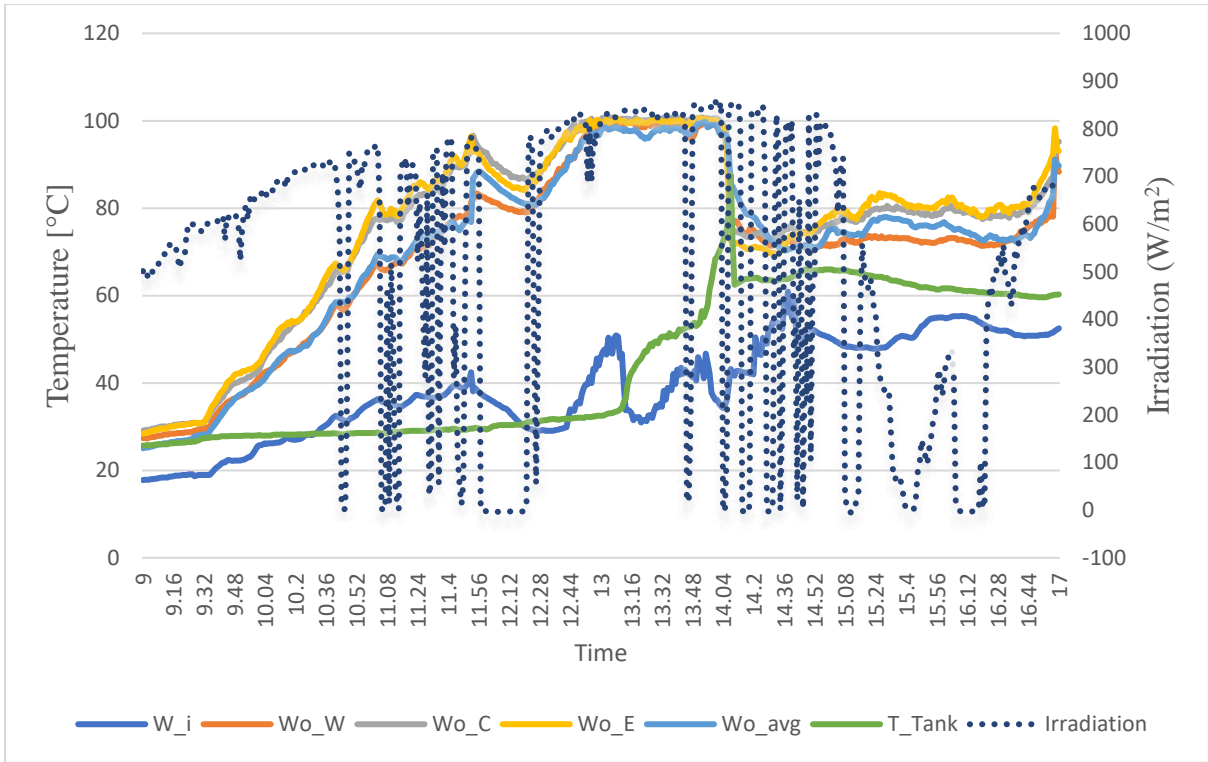


Figure 4.2: Variation of Water Inlet Temperature, Water outlet Temperature and Water Temperature in Tank with Time on 13th February.

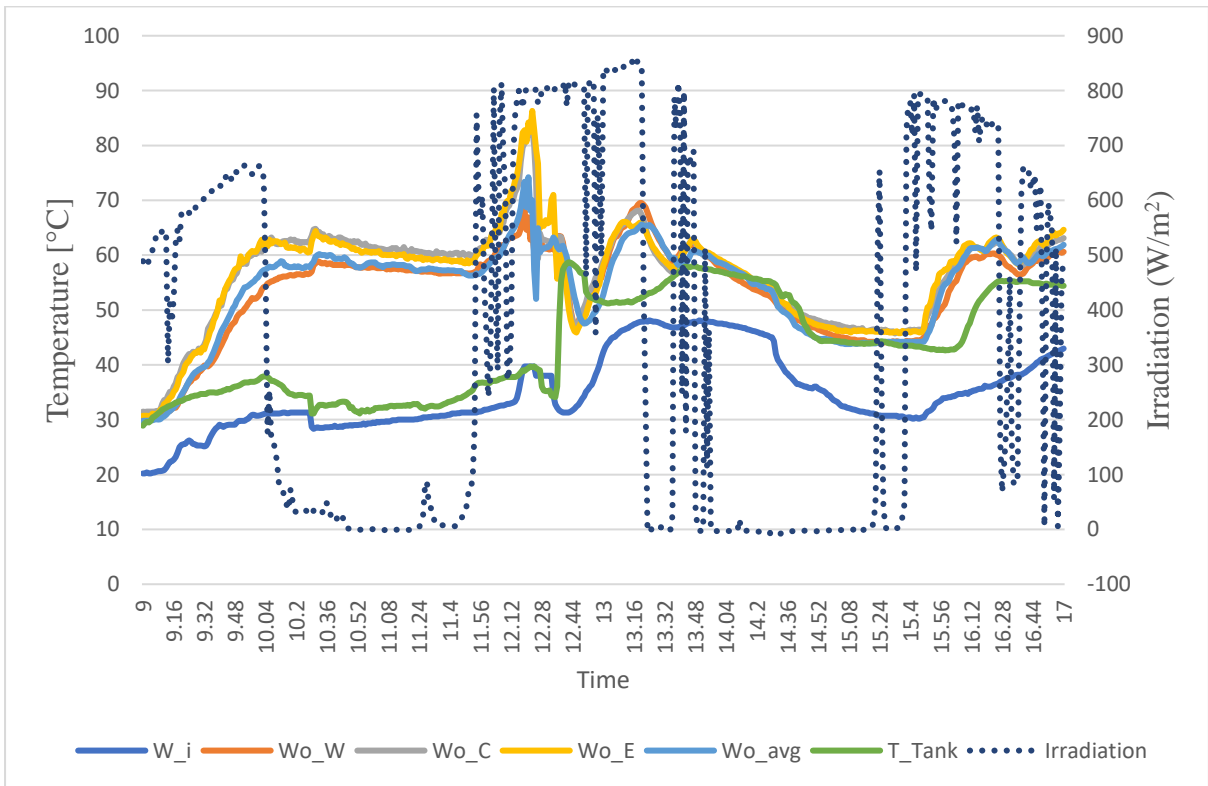


Figure 4.3: Variation of Water Inlet Temperature, Water outlet Temperature and Water Temperature in Tank with Time on 14th February.

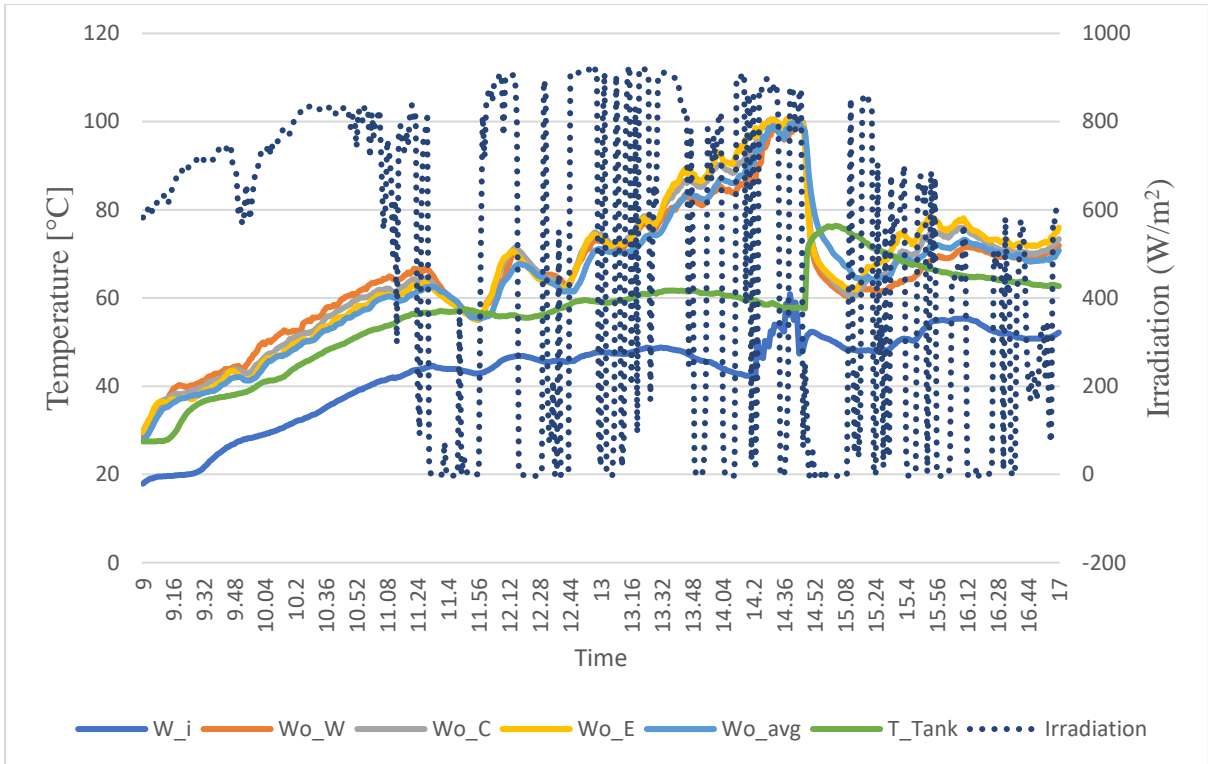


Figure 4.4: Variation of Water Inlet Temperature, Water outlet Temperature and Water Temperature in Tank with Time on 16th February.

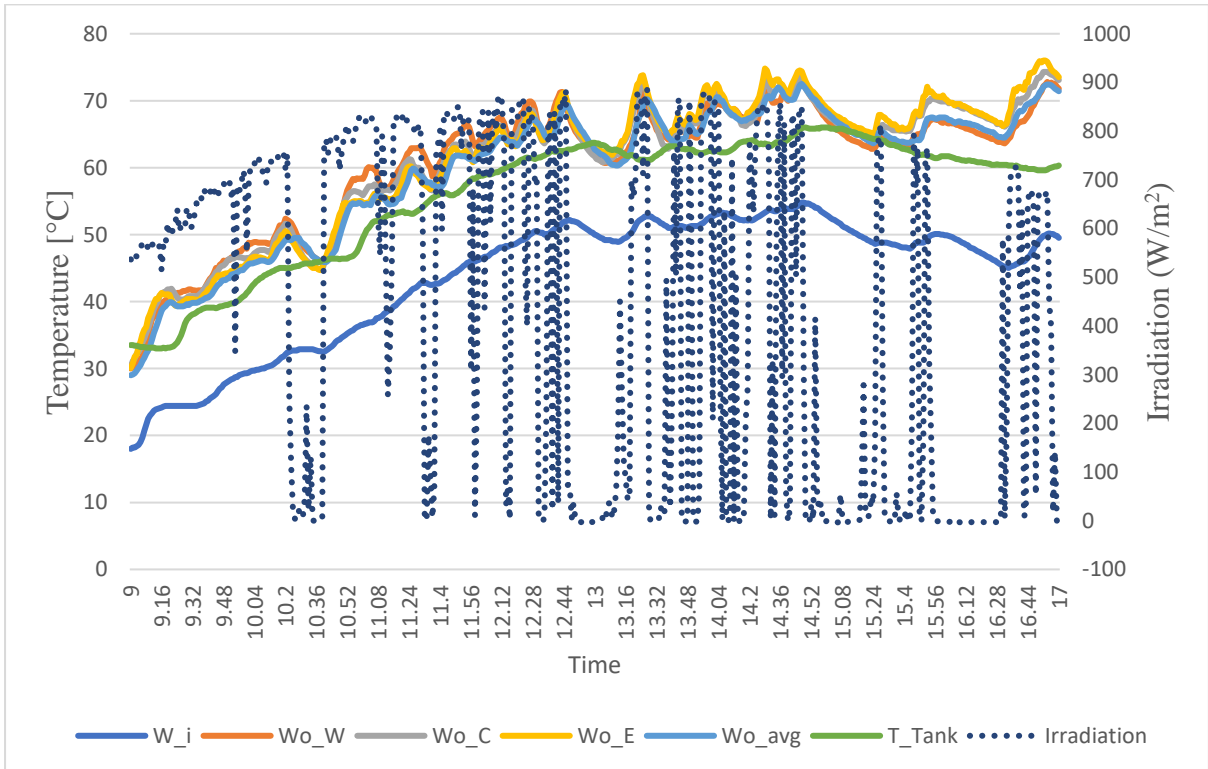


Figure 4.5: Variation of Water Inlet Temperature, Water outlet Temperature and Water Temperature in Tank with Time on 17th February.

4.2 Estimated Power Absorbed by Water

The flow rate of water in the vertically oriented CPC collector was unable to be determined because of financial and time constraints. Flow rate is vital to determine the instantaneous power absorbed by the working fluid by using heat transfer equation. An estimated flow rate of 0.001 kg/s and 0.002 kg/s was used as the range of mass flow rate of 90° mounted CPC collector are within the proposed value used in the calculation. Instantaneous power absorbed for water's mass flow rate at 0.001 kg/s and 0.002 kg/s on 13th, 14th, 16th and 17th February are presented on Figure 4.6, Figure 4.7, Figure 4.8 and Figure 4.9. Figure 4.10 depicts the expected cumulative power absorbed for water's mass flow rate at 0.001 kg/s and 0.002 kg/s on 13th, 14th, 16th and 17th February.

The maximum power absorbed for mass flow rate of 0.001 kg/s is approximately 273 W whereas the cumulative power absorbed on each experimental day can reach up to 0.7 MW. Furthermore, the maximum power absorbed for mass flow rate of 0.002 kg/s is estimated to be 557 W whereas the cumulative power absorbed on each experimental day can reach up to 1.3 MW.

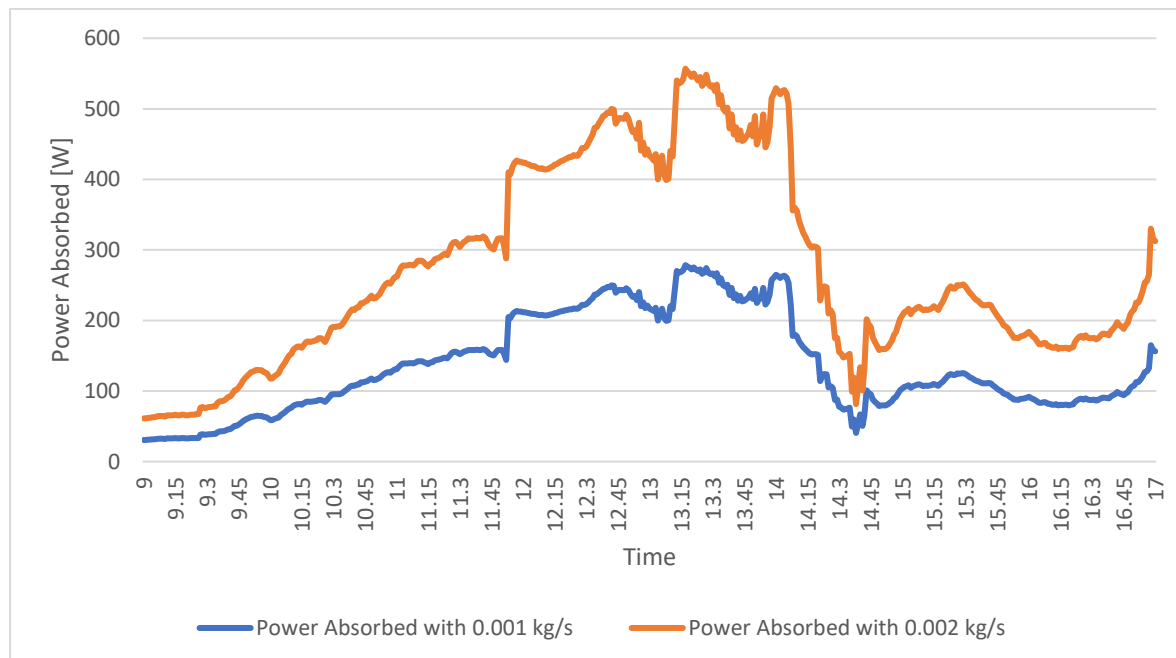


Table 4.6: Estimated Instantaneous Power Absorbed on 13th February with Water's Mass Flow Rate of 0.001 kg/s and 0.002 kg/s

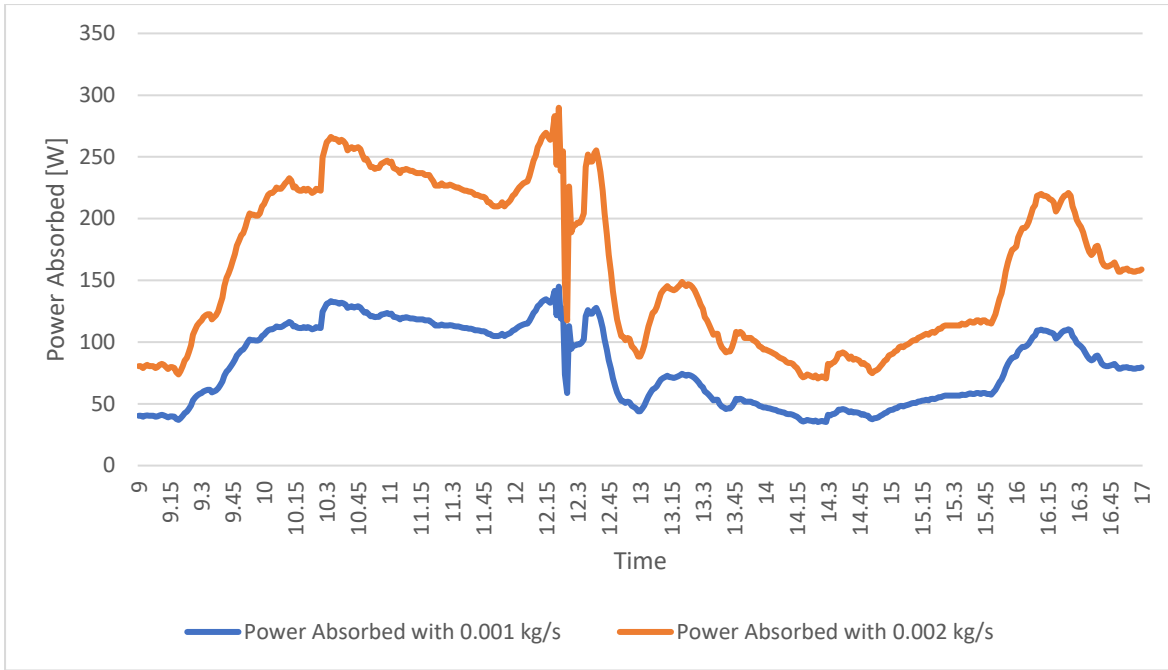


Table 4.7: Estimated Instantaneous Power Absorbed on 14th February with Water’s Mass Flow Rate of 0.001 kg/s and 0.002 kg/s

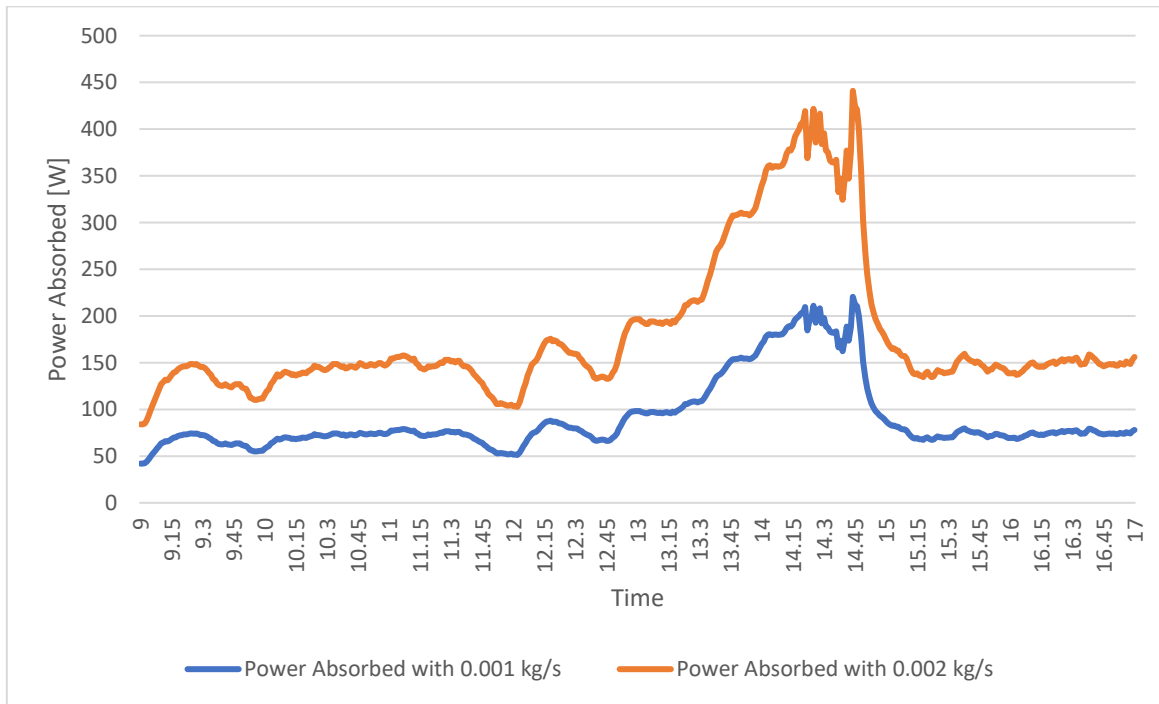


Table 4.8: Estimated Instantaneous Power Absorbed on 16th February with Water’s Mass Flow Rate of 0.001 kg/s and 0.002 kg/s

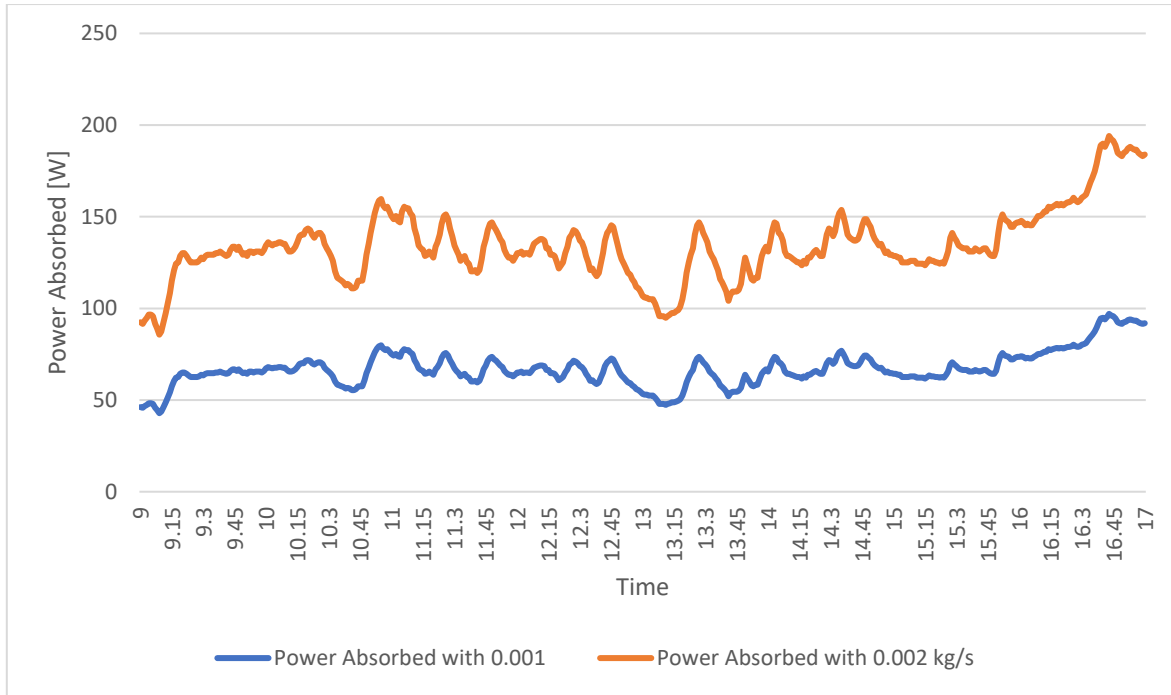


Table 4.9: Estimated Instantaneous Power Absorbed on 17th February with Water’s Mass Flow Rate of 0.001 kg/s and 0.002 kg/s

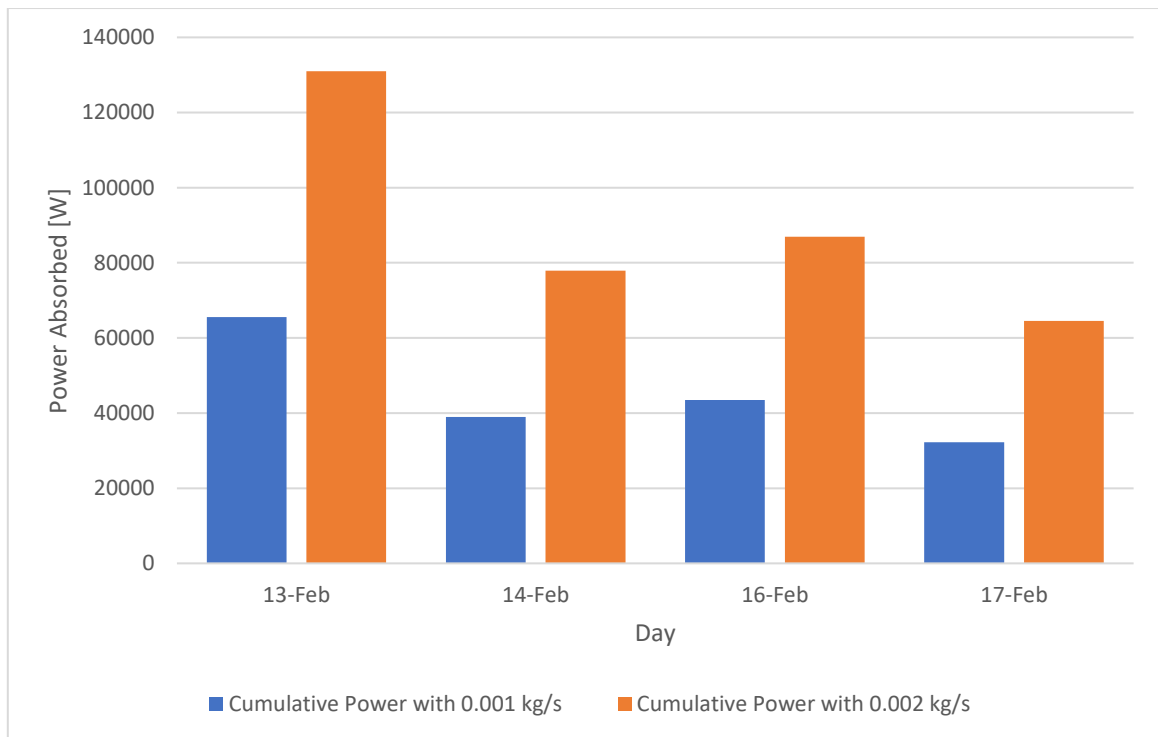


FIGURE 4.10: Cumulative Power Absorbed by the CPC Collector with Water’s Mass Flow Rate of 0.001 kg/s and 0.002 kg/s

4.3 Thermal Efficiency

The maximum average thermal efficiency for mass flow rate of 0.001 kg/s is approximately 6% whereas The maximum average thermal efficiency for mass flow rate of 0.002 kg/s is approximately 12%. The mass flow rate (m) is the function of useful energy (Q_u). Low efficiency obtained because small mass flow rate present in the system. Total power received by CPC collector (Q_{in}) was from primary receiver namely west heliostat, centre heliostat and east heliostat.

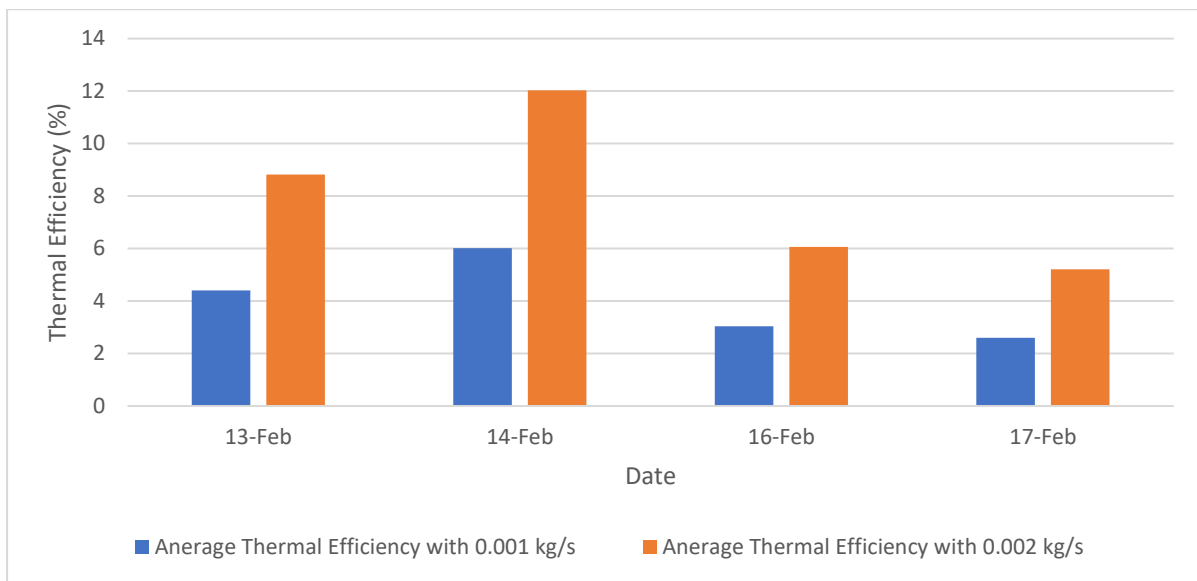


Figure 4.11: Average Thermal Efficiency of CPC Collector with Water's Mass Flow Rate of 0.001 kg/s and 0.002 kg/s

CHAPTER 5

CONCLUSION AND RECOMMENDATION

5.1 Conclusion

Based on this research work, the thermal performance evaluation of vertically oriented CPC collector requires procedures to be complied strictly in order to obtain effective results. Furthermore, testing on CPC collector mounted at 90° angle is a good research in order to create a valuable reference for future developments and possibilities in improving the future thus minimize the space requirement for mounting thermal solar collectors by solar industry. The water outlet temperature can reach up to 50°C on a day with high solar radiation when the collector is not integrated with heliostat field but the concept of thermosiphoning is not feasible as there is no change in water tank temperature throughout the day. The water outlet temperature can reach up to 101°C on a day with high solar radiation whereas 76°C on a day with low solar radiation when being integrated with heliostat field which results such system can be employed for high thermal application in locations such heavy industries as water temperature went up above boiling point where steam is generated. The inclination angle is not at all affecting the thermosyphon movement of water inside the CPC collector when integrated with heliostat field. Pumping power can be significantly saved as the system able to be operated by means of natural circulation. Despite all the advantage, on drawback of the CPC collector when mounted in 90° is that low power absorbed on a day with low solar radiation as the amount of power absorbed depends on intensity of solar radiation and number of heliostats employed. The output of the undertaken project will be very useful for researchers to further enhance its efficiency.

5.2 Recommendations

Optical efficiency, working fluid and heat loss to surrounding are the main factor that contribute to low power absorption by the vertically oriented CPC collector when integrated with heliostat. Large gap between the glass tube and absorber tube contribute to major gap loss that minimize the extent of solar radiation to reach the surface of the absorber tube. The absorber tube should be redesigned in subsequent experiment for better optical efficiency that contribute to higher value of thermal efficiency.

Heat transfer fluid (HTF) plays a vital role in evaluating the efficiency of the solar energy utilization. Water is chosen in this experiment as it is nontoxic and inexpensive. In subsequent experiment thermal oil can be used since CPC collector and heliostat field were intended for medium and high thermal application. Thermal oils generally have high thermal limit.

Sun tracer should be equipped for every dual-axis heliostat in Universiti Teknologi PETRONAS. Currently UTP is developing automated heliostat field which uses open-loop control technique which uses microprocessor which programmed such that it can determine position of sun at any time. Such technology should be employed to harness maximum possible solar energy thus directing it to central receiver. Currently UTP is developing automated heliostat field which uses open-loop control technique which uses microprocessor which programmed such that it can determine position of sun at any time. Such technology should be employed to harness maximum possible solar energy thus directing it to central receiver.

REFERENCES

- [1] Goswami, D.Y., 2015. Principles of Solar Engineering. 3rd ed. Boca Raton: Taylor & Francis Group
- [2] “Solar Water Heating: A Comprehensive Guide to Solar Water and Space Heating Systems by Bob Ramlow,” *Goodreads*, 01-Jun-2006. [Online]. Available: https://www.goodreads.com/book/show/175797.Solar_Water_Heating.
- [3] W. J. Makofske, “Renewing with Renewables: Direct Solar Energy Use in Developing Countries,” *Disaster by Design: The Aral Sea and its Lessons for Sustainability Research in Social Problems and Public Policy*, pp. 357–371, 2012.
- [4] S. A. Kalogirou, “Solar thermal collectors and applications,” *Progress in Energy and Combustion Science*, vol. 30, no. 3, pp. 231–295, 2004
- [5] M. Sabiha, R. Saidur, S. Mekhilef, and O. Mahian, “Progress and latest developments of evacuated tube solar collectors,” *Renewable and Sustainable Energy Reviews*, vol. 51, pp. 1038–1054, 2015.
- [6] S. A. Waghmare and N. P. Gulhane, "Design and ray tracing of a compound parabolic collector with tubular receiver," *Solar Energy*, vol. 137, pp. 165-172, 2016.
- [7] A. Alamoudi, S. M. Saaduddin, A. B. Munir, F. Muhammad-Sukki, S. H. Abu-Bakar, S. H. M. Yasin, R. Karim, N. A. Bani, A. A. Mas’Ud, J. A. Ardila-Rey, R. Prabhu, and N. Sellami, “Using Static Concentrator Technology to Achieve Global Energy Goal,” *Sustainability*, vol. 11, no. 11, p. 3056, 2019
- [8] S. H. Abu-Bakar, F. Muhammad-Sukki, R. Ramirez-Iniguez, T. K. Mallick, A. B. Munir, S. H. M. Yasin, and R. A. Rahim, “Rotationally asymmetrical compound parabolic concentrator for concentrating photovoltaic applications,” *Applied Energy*, vol. 136, pp. 363–372, 2014.
- [9] Y. Su, G. Pei, S. B. Riffat, and H. Huang, “Radiance/Pmap simulation of a novel lens-walled compound parabolic concentrator (lens-walled CPC),” *Energy Procedia*, vol. 14, pp. 572–577, 2012.
- [10] L. Guiqiang, P. Gang, S. Yuehong, W. Yunyun, and J. Jie, “Design and investigation of a novel lens-walled compound parabolic concentrator with air gap,” *Applied Energy*, vol. 125, pp. 21–27, 2014
- [11] R. Winston, L. Jiang, and B. Widyolar, “Performance of a 23KW Solar Thermal Cooling System Employing a Double Effect Absorption Chiller and

- Thermodynamically Efficient Non-tracking Concentrators,” *Energy Procedia*, vol. 48, pp. 1036–1046, 2014
- [12] M. Tian, Y. Su, H. Zheng, G. Pei, G. Li, and S. Riffat, “A review on the recent research progress in the compound parabolic concentrator (CPC) for solar energy applications,” *Renewable and Sustainable Energy Reviews*, vol. 82, pp. 1272–1296, 2018.
- [13] Y. Kim, G. Han, and T. Seo, “An evaluation on thermal performance of CPC solar collector,” *International Communications in Heat and Mass Transfer*, vol. 35, no. 4, pp. 446–457, 2008.
- [14] H. Zheng, “Solar Energy Utilization and Its Collection Devices,” *Solar Energy Desalination Technology*, pp. 47–171, 2017.
- [15] J. A. Duffie and W. A. Beckman, "Solar engineering of thermal processes," 1980.
- [16] R. Tang and T. Wu, "Optimal tilt-angles for solar collectors used in China," *Applied Energy*, vol. 79, pp. 239-248, 2004.
- [17] E. A. Handoyo, D. Ichsani, and Prabowo, "The Optimal Tilt Angle of a Solar Collector," *Energy Procedia*, vol. 32, pp. 166-175, 2013.
- [18] T. Khatib, A. Mohamed, and K. Sopian, "On the monthly optimum tilt angle of solar panel for five sites in Malaysia," in *2012 IEEE International Power Engineering and Optimization Conference Melaka, Malaysia*, pp. 7-10, 2012
- [19] M. Alghoul, M. Sulaiman, B. Azmi, and M. Wahab, “Review of materials for solar thermal collectors,” *Anti-Corrosion Methods and Materials*, vol. 52, no. 4, pp. 199–206, 2005.
- [20] D. Barlev, R. Vidu, and P. Stroeve, “Innovation in concentrated solar power,” *Solar Energy Materials and Solar Cells*, vol. 95, no. 10, pp. 2703–2725, 2011.